THESIS

INTEGRATED AQUIFER CHARACTERIZATION IN THE PAROWAN VALLEY WITH DRILLERS' LOGS AND TRANSIENT ELECTROMAGNETIC SYSTEMS

Submitted by

Kendra Bratzler

Department of Civil and Environmental Engineering

In partial fulfillment of requirements

For the Degree of Master of Science

Colorado State University

Fort Collins, Colorado

Summer 2026

Master's Committee:

Advisor: Ryan G. Smith

Ryan Bailey
Lisa Stright

ABSTRACT

INTEGRATED AQUIFER CHARACTERIZATION IN THE PAROWAN VALLEY WITH DRILLERS' LOGS AND TRANSIENT ELECTROMAGNETIC SYSTEMS

The Parowan Valley in southwestern Utah is an agricultural region that has experienced significant land subsidence in recent years due to excessive groundwater pumping. Subsidence occurs primarily in regions containing fine-grained materials such as clay deposits, making accurate characterization of subsurface lithology critical for informing groundwater management strategies aimed at mitigating further subsidence.

Previous subsurface characterization efforts have relied on either geophysical data or directly sampled lithologic data independently. This study integrates both datasets to improve subsurface characterization within Parowan Valley. Transient electromagnetic (TEM) measurements collected using tTEM and WalkTEM systems provide spatially extensive electrical resistivity data and offer a faster, more cost-effective alternative to direct sampling methods. However, converting resistivity to lithology requires a rock physics transform and is strongly influenced by subsurface saturation conditions. To address this, monitoring well data were used to estimate depth to groundwater throughout the study area using cokriging with land surface elevation as a secondary variable. Direct lithologic observations were obtained from drillers' logs, which provide subsurface material descriptions but are subject to inconsistencies due to an absence of standardized reporting practices.

The geophysical and lithologic datasets were integrated and interpolated using ordinary kriging. Model performance was evaluated using held-out drillers' logs to assess interpolation accuracy and optimize resistivity thresholds for saturated and unsaturated coarse-grained and fine-grained materials. Results demonstrate that integrating geophysical, lithologic, and hydrologic datasets improves subsurface characterization relative to interpolation performed using lithologic observations alone. The resulting interpolated fraction of coarse-grained material maps provide insight into the spatial distribution of clay deposits and may support groundwater management efforts in regions vulnerable to land subsidence.

ACKNOWLEDGEMENTS

I would like to acknowledge and thank the many people and organizations who made this research possible. First and foremost, thank you to my advisor, Dr. Ryan Smith, for his support, guidance, and feedback throughout this project. I truly could not have asked for a better advisor and am extremely thankful that he decided to take a chance on me as an incoming graduate student so that I could pursue my passion for groundwater hydrology. Additionally, thank you to Dr. Ryan Bailey and Dr. Lisa Stright for serving on my committee and providing valuable insights.

A week-long field campaign in the Parowan Valley allowed for the collection of WalkTEM data that was instrumental to the success of this project. This work would not have been possible without the field team, comprised of Dr. Erich Mueller, Devon Fischer, Moira Straga, and Gibson Bezoski from Southern Utah University, Kayla Smith and Noah Christensen from the Utah Geological Survey, and Dr. Jiawei Li from Colorado State University. A special thank you to Jason Bradshaw from the United States Department of Agriculture whose coordination with the Parowan Valley community was instrumental in securing land access for the field campaign. My thanks also go to Dr. Bradley James Carr from the University of Wyoming for providing WalkTEM system training prior to the field campaign and offering guidance on data processing afterwards. I would also like to thank Zoe Vanderwal for her help in reviewing and analyzing hundreds of drillers' logs, an effort that was extremely valuable to this project.

I am extremely thankful for the Remote Sensing Hydrology Research Group led by Dr. Ryan Smith, composed of Dr. Soheil Nozari, Dr. Jiawei Li, Fahim Hasan, Abdullah Al Fatta, Rahel Pommerenke, Dawit Asfaw, Julianne Robinson, Susmita Pant, Dana Rastad, and Colton Ward. The camaraderie within this group made my graduate experience incredibly memorable, and I hope every graduate student is fortunate enough to find a lab group as special as this one.

I am also grateful to the donors of the scholarships I received during my time at Colorado State University: the Whitney Borland Scholarship and the Civil and Environmental Engineering Department Scholarship. Their generous support made both this research and my graduate education possible.

Finally, I would like to thank my friends and family for their encouragement throughout my graduate school journey. Specifically, thank you to my mother, Suzanna, and father, David, for instilling in me, from a young age, the confidence to pursue my dreams.

TABLE OF CONTENTS

LIST OF TABLES

LIST OF FIGURES

1. INTRODUCTION

1.1 Background

Overextraction of groundwater resources in agricultural regions can contribute to land subsidence due to compaction of fine-grained materials (Bouwer, 1977). This land subsidence can have devastating impacts on infrastructure, both underground and on the surface, in addition to the development of earth fissures (Conway, 2016). Identifying the spatial distribution of fine-grained materials can support groundwater management decisions by highlighting regions more susceptible to compaction and land subsidence.

As an agricultural region in southwestern Utah, Parowan Valley relies heavily on groundwater and has experienced significant land subsidence due to overextraction of these resources. Therefore, locating fine-grained material deposits is of interest to the community, and geophysical data provides a fast, cost-effective, and noninvasive method for doing so. However, geophysical measurements of electrical resistivity do not directly represent lithology and therefore require transformation approaches that introduce uncertainty. In contrast, directly sampled drillers' logs provide lithologic observations without requiring resistivity transformations. However, the absence of standardized reporting practices and the low priority placed on lithologic classification for most wells drilled results in significant inconsistencies and inaccuracies across logs. Additionally, the time and cost intensive nature of direct sampling often leads to sparse spatial data coverage. To address the limitations of both datasets, this study introduces an integrated interpolation approach combining geophysical resistivity data with directly sampled lithologic observations.

Accurate subsurface characterization using both geophysical and lithologic datasets may reduce the need for extensive direct sampling while improving spatial understanding of fine-grained deposits. This is particularly important in regions experiencing groundwater depletion and land subsidence, where timely subsurface characterization can support more sustainable groundwater management practices.

1.2 Research Gap

Geophysical methods including ground penetrating radar (GPR), electrical resistivity tomography (ERT), and electromagnetic (EM) surveys are widely used for groundwater and subsurface investigations. Numerous studies have integrated EM measurements with borehole or lithologic observations to improve subsurface interpretation. For example, Knight et al. (2018) established quantitative relationships between airborne electromagnetic (AEM) data and drillers' logs to transform resistivity models into hydrostratigraphic interpretations, while explicitly accounting for saturated and unsaturated conditions. Sandersen et al. (2021) and Maurya et al. (2020) demonstrated the value of visually comparing borehole logs and tTEM data for detailed geological mapping, while Nugroho et al. (2023) used borehole logs in a machine learning algorithm approach to enhance lithologic mapping. Collectively, these studies demonstrate that integrating EM and lithologic data is an established approach for improving subsurface characterization.

Within Parowan Valley, previous studies have similarly applied a variety of geophysical and lithologic datasets to investigate groundwater depletion, land subsidence, and subsurface conditions. Interferometric synthetic aperture radar (InSAR) has been used to estimate aquifer storage loss (Smith et al., 2023), while mapping of ground fissures has identified regions experiencing consolidation of fine-grained deposits (DuRoss & Kirby, 2004). Additional work utilized drillers' logs to generate lithologic cross-sections (Li et al., 2023), while more recent studies have applied rock physics transformations to tTEM data to estimate subsurface lithology from electrical resistivity measurements (Li et al., 2024).

Despite these advances, both within the broader literature and in Parowan Valley specifically, lithologic observations are commonly used to constrain, calibrate, interpret, or validate geophysical models (King & González-Álvarez, 2016; Sandersen et al., 2021; Maurya et al., 2020; Baines et al., 2002; Auken et al., 2018), after which the final characterization relies primarily on the geophysical dataset (Knight et al., 2018; Li et al., 2024; Nugroho et al., 2023; Gorrie et al., 2025; Muhammad et al., 2022). Among the studies reviewed, Nugroho et al. (2023) comes closest to retaining lithologic observations within the final classification by training a machine learning model using borehole logs. However, once trained, the model predicts lithology exclusively from geophysical inputs, meaning borehole logs no longer directly contribute to the final lithologic classification. Consequently, comparatively little attention has been given to approaches that retain both geophysical and lithologic observations as active inputs within a unified interpolation framework while quantitatively evaluating the benefit of that integration. Additionally, uncertainty associated with transforming electrical resistivity to lithology under varying saturation conditions remains insufficiently explored. This study addresses these gaps by integrating EM-derived lithologic estimates and directly sampled lithologic observations within an ordinary kriging framework and evaluating the performance of the integrated approach using independent held-out data.

1.3 Research Objectives

The objective of this study is to develop and evaluate an integrated interpolation approach that combines geophysical resistivity data with directly sampled lithologic observations to improve subsurface characterization within Parowan Valley. Electrical resistivity measurements collected using the tTEM and WalkTEM systems are utilized as proxies for lithology, with explicit consideration given to the influence of subsurface saturation on resistivity response. Interpolation results from the integrated approach are compared against interpolation performed using lithologic observations alone to evaluate the added value of geophysical data integration. Ultimately, this study aims to produce improved interpolated fraction of coarse-grained material maps to improve characterization of groundwater flow, subsidence risk, and to support sustainable groundwater management decisions within Parowan Valley.

2. METHODOLOGY

2.1 Study Area

The study area is located in Parowan Valley in southwestern Utah, an agricultural region in Iron County that includes the towns of Parowan, Paragonah, and Summit (Figure 1). The valley is characterized as a predominantly closed basin, with limited surface outflow at its southwestern end through Winn Gap into Cedar Valley (Marston, 2017). Most surface water within the basin drains toward the Little Salt Lake, which consists of fine-grained lacustrine deposits. The lake has largely diminished, likely due to reduced recharge associated with sustained groundwater extraction (Smith & Li, 2021).

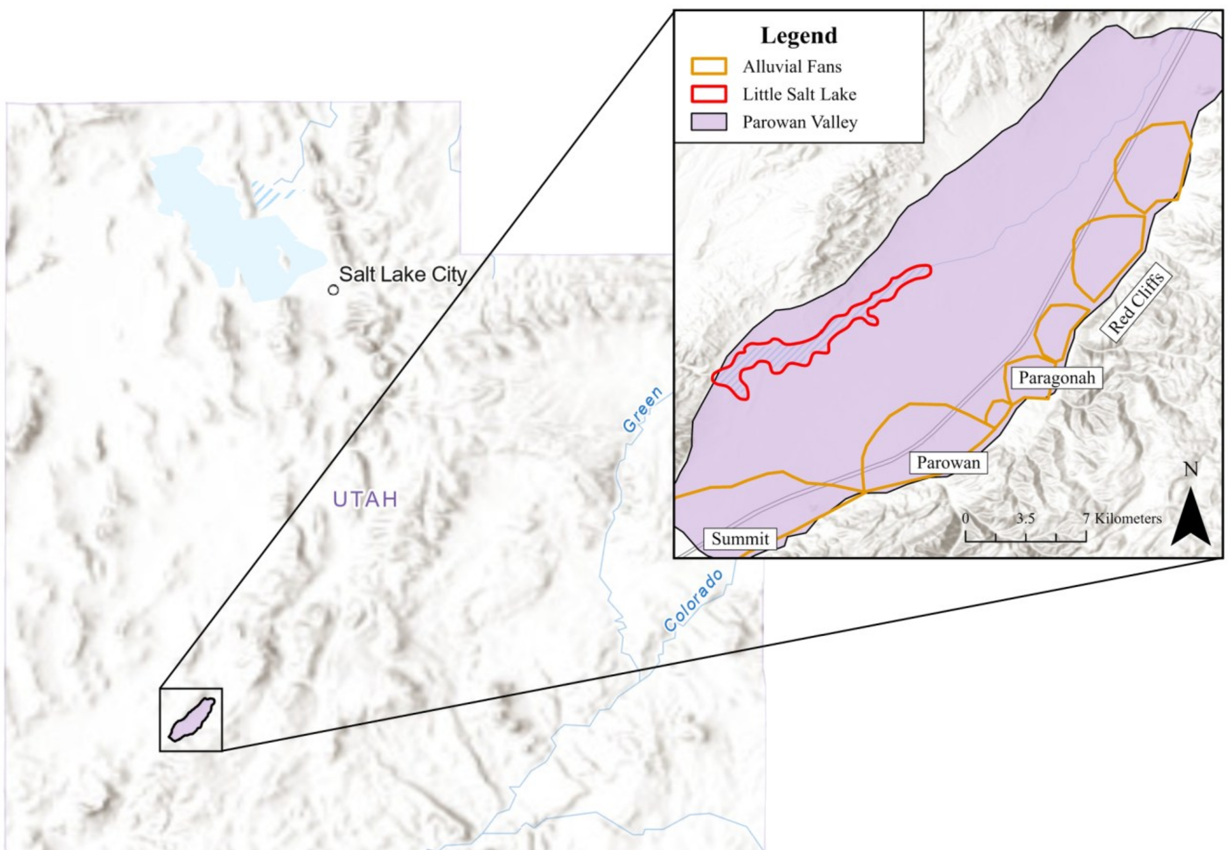

Figure 1: Parowan Valley Study Area

Recharge to the basin is primarily derived from the southeastern Red Cliffs, where coarse-grained alluvial fan deposits occur along the base. This contrast between coarse-grained recharge zones and fine-grained basin-center deposits plays an important role in controlling groundwater flow and storage within the valley.

This hydrogeologic setting has important implications for groundwater use and land stability. Overextraction of groundwater from the unconsolidated basin-fill aquifer has resulted in significant land subsidence, with approximately 30 cm of displacement observed between 2014 and 2020 (Li et al., 2023). Groundwater resources in Parowan Valley are heavily utilized for agriculture, particularly in the northwestern portion of the basin where fine-grained deposits are prevalent (Marston, 2017). As a result, effective groundwater management is critical for maintaining the long-term economic sustainability of the region, which relies on continued use of local water resources.

2.2 Data Sources

2.2.1 Groundwater Level Data

A total of 167 monitoring wells within the study area were obtained from the Utah Division of Water Rights (https://waterrights.utah.gov/). This dataset includes both United States Geological Survey (USGS) wells and privately operated agricultural wells that report data to the Utah Division of Water Rights (UDWR). Groundwater levels, reported as depth to groundwater (DTGW), are typically measured in March. However, measurements are not consistently recorded on an annual basis for all wells. Well depth information is available for the majority of USGS monitoring wells but is not reported for wells operated by UDWR. Figure A1 in Appendix A shows the spatial distribution of monitoring wells. To illustrate recent sampling density, wells are color coded according to the number of groundwater level measurements collected since 2020.

2.2.2 Lithologic Data

A total of 194 drillers' logs within the study area were obtained from the Utah Division of Water Rights (https://waterrights.utah.gov/). Well drilling has been conducted by different companies using various methods over the past 150 years, resulting in substantial variability in both the format and quality of the logs. This variability reflects the absence of standardized reporting practices for drillers' logs in Utah. Due to inconsistencies in lithologic descriptions across the dataset, variably reported lithology from drillers' logs was generalized into three categories: fine-grained, coarse-grained, and mixed-grained (see Li et al., 2024 for details on classification). The spatial distribution of drillers' logs is shown in Figure 2.

2.2.3 Geophysical Data

A total of 104.7 km of tTEM data was collected across the study area in November 2021 over a two-day period. Details of the tTEM system, survey design, and data processing are provided in Li et al. (2024). This dataset is split into two groups, one over the Little Salt Lake and the remaining data in the northeast and southwest regions of the study area. In addition, 33 WalkTEM soundings were acquired in October 2025 over five days. Because the WalkTEM data were collected after the tTEM survey, acquisition efforts were focused on regions with sparse tTEM coverage and limited drillers' log data to improve spatial coverage across the study area. The spatial distribution of both geophysical datasets is shown in Figure 2.

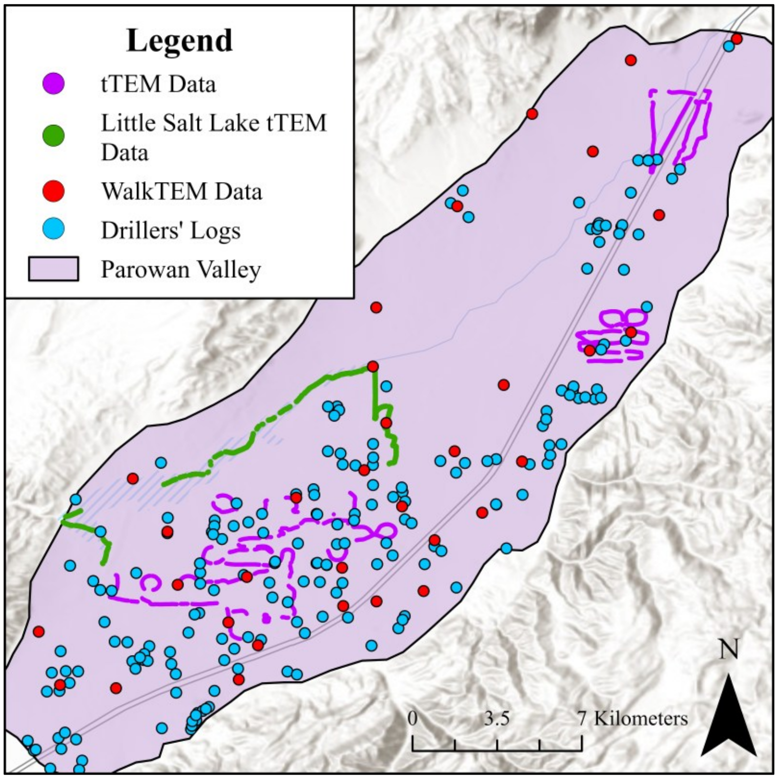

Figure 2: Geophysical Datasets and Drillers' Logs

2.3 Data Processing

2.3.1 Water Table Delineation for Degree of Saturation Modeling

Geophysical data report electrical resistivity, a parameter that is strongly influenced by subsurface saturation (McCarter, 1984). Therefore, accurate delineation of the water table is required to estimate degree of saturation and apply a robust rock physics transform. Most groundwater level measurements in Parowan Valley are collected in March, but an unusually extensive dataset from November 2012 is available and was selected as the reference condition because it aligns seasonally with geophysical data acquired in November 2021 (tTEM) and October 2025 (WalkTEM). The analysis proceeded in three steps: (1) identify monitoring wells that tap the upper unconfined aquifer so that measured water levels represent the water table rather than a confined potentiometric surface, (2) use those wells together with land surface elevation to generate a November 2012 DTGW surface by cokriging, and (3) transform the November 2012 DTGW surface to estimate November 2021 and November 2025 conditions while accounting for both intraseasonal and interannual changes. Because the WalkTEM data was acquired in October 2025, but groundwater level measurements were unavailable for that month, the November 2025 DTGW surface was used as a reasonable approximation, assuming minimal groundwater level change between October and November.

2.3.2 Aquifer Compartmentalization

Due to the absence of mapped confining layers within Parowan Valley, it was necessary to evaluate the presence of vertically distinct aquifer systems to ensure that measured water levels represent the water table rather than the potentiometric surface of a confined aquifer. Misrepresentation of potentiometric head as the water table would result in overestimation of the saturated zone. To address this, the November 2012 monitoring wells were grouped by well depth into three categories: shallow (0 - 100 m), medium (100 - 200 m), and deep (200 - 300 m).

The relationship between DTGW and well depth, found in Figure A2 in Appendix A, reveals that several deep wells exhibit relatively shallow water levels despite well depths exceeding 200 m. Deeper wells can be correlated with more confined conditions (Hilton & Jasechko, 2023). While deep wells with shallow DTGW measurements can occur in unconfined aquifers, such conditions can also be indicative of a confined aquifer system.

The presence of multiple aquifers often causes significant discontinuities in DTGW measurements of nearby wells. Spatial mapping of DTGW by well depth group, however, does not reveal any abrupt or anomalous transitions between neighboring values as seen in Figure A3 in Appendix A. Instead, DTGW measurements from shallow, medium, and deep wells appear to vary smoothly across the study area, which could be interpreted as indicative of a hydraulically connected system.

However, when considered alongside the DTGW versus well depth relationship, where several deep wells exhibit relatively shallow water levels, there remains the possibility that some deeper wells are influenced by confined conditions and therefore reflect potentiometric surface elevations rather than the water table. Because the dataset does not include screen interval information, it is not possible to definitively determine which wells may be affected.

Continuing the analysis of potential aquifer differentiation, the drillers' log dataset was examined for indicators of confined conditions. A "Static Water Level / Water Level Data" section present in several logs was used to identify flowing artesian wells. A total of three flowing wells, documented between 2001 and 2003, were identified and all fall within the medium depth category (100 - 200 m). These flowing wells are mapped in Figure A4 in Appendix A while the corresponding drillers' logs can be found in Figure C1 through Figure C5 in Appendix C.

Flowing artesian conditions indicate that groundwater is under sufficient pressure for hydraulic head to rise above the land surface, which is characteristic of confined aquifers. The occurrence of flowing wells exclusively within the medium depth range suggests that wells of this depth may intersect a confined system in parts of the study area.

Although only a limited number of flowing wells were identified, this observation, combined with the absence of screen interval data and the previously noted ambiguity in DTGW patterns, introduces uncertainty regarding whether medium and deep wells consistently represent the water table or a potentiometric surface. Evidence of a confining unit near the center of Parowan Valley, likely associated with fine-grained materials historically deposited in the Little

Salt Lake (Li et al., 2023), further supports the possibility of confined conditions within portions of the aquifer system and adds to the uncertainty surrounding medium and deep wells. To minimize the risk of incorporating potentiometric surface measurements from confined aquifers into the interpolation of the water table, a conservative approach was adopted in which medium (100 - 200 m) and deep (200 - 300 m) wells were excluded from the November 2012 monitoring wells dataset. This ensures that the resulting surface is more likely to reflect unconfined conditions, although at the cost of reduced spatial coverage.

2.3.3 Interpolated Water Levels

Following the exclusion of medium and deep wells, only shallow monitoring wells (0 - 100 m) from the November 2012 dataset were used to interpolate DTGW across the study area. Cokriging was implemented in ArcGIS Pro, using DTGW as the primary variable and land surface elevation derived from USGS digital elevation models (DEMs) as the secondary variable. A smooth search neighborhood was selected, which uses three concentric ellipses and applies a gradual reduction in weighting with increasing distance from the prediction location. Because only 19 shallow wells were available, the major and minor semiaxes were expanded to 15,000 m for the primary variable and 21,000 m for the secondary variable to ensure that all observations could contribute to each prediction. A smoothing factor of 0.2 was applied so that wells located farther from the prediction location received progressively lower weights through a sigmoidal weighting function (Esri, 2026). This relatively low smoothing factor allowed all available observations to contribute to the interpolation while maintaining stronger influence from nearby wells and preserving regional groundwater trends.

The resulting cokriging surface was extended to the full extent of the Parowan Valley study area to provide complete spatial coverage for subsequent integration with geophysical datasets (Figure 3). However, because predictions beyond the spatial extent of the November 2012 monitoring wells are less constrained by observed data, DTGW estimates in the southwest and northeast corners of the study area should be interpreted with caution. Despite this uncertainty, the very shallow DTGW in the north-central portion of the study area coincides with the location of Wheatgrass Springs (Marston, 2017), providing an independent hydrogeologic explanation for the near-surface groundwater predicted by the cokriging surface.

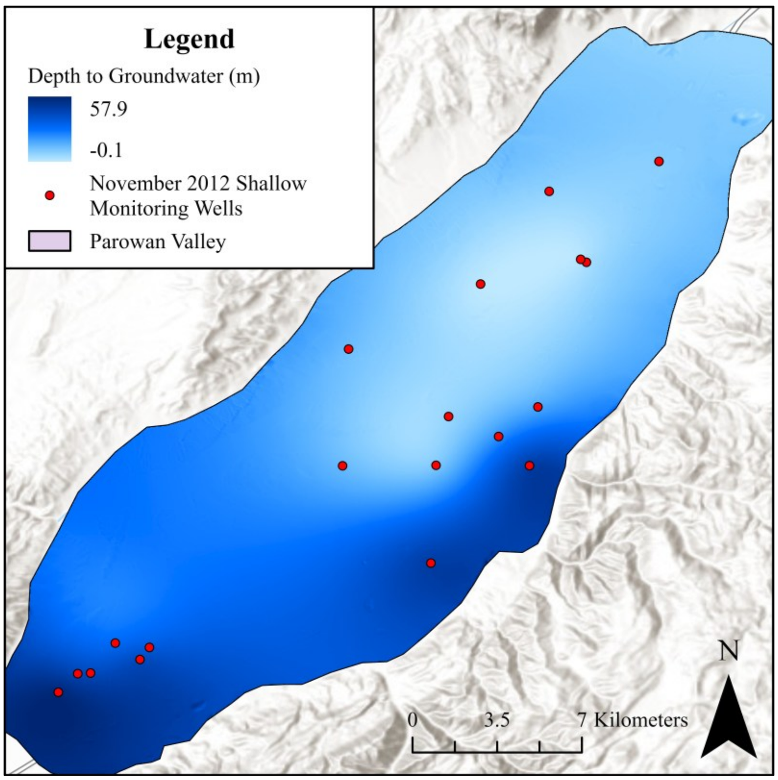

Figure 3: Depth to Groundwater with November 2012 Shallow Monitoring Wells

To align subsurface saturation conditions with geophysical data acquisition dates, the November 2012 DTGW surface was temporally adjusted to estimate DTGW conditions for November 2021 and November 2025. Because monitoring well datasets corresponding directly to these two periods were unavailable, an indirect estimation procedure was required. Paired

March 2012 and November 2012 DTGW measurements were used to calculate a seasonal difference (Eq. (1)).

$$Seasonal\ Difference = DTGW_{November\ 2012} - DTGW_{March\ 2012} \tag{1}$$

These seasonal differences were then added to March 2021 and March 2025 DTGW measurements to estimate corresponding November conditions (Eq. (2) and Eq. (3)).

$$Estimated\ DTGW_{November\ 2021} = DTGW_{March\ 2021} + Seasonal\ Difference \tag{2}$$

$$Estimated\ DTGW_{November\ 2025} = DTGW_{March\ 2025} + Seasonal\ Difference \tag{3}$$

Application of this approach required a monitoring well to have measurements from November 2012, March 2012, and either March 2021 or March 2025. Consequently, only shallow monitoring wells (0 - 100 m) meeting these criteria could be used to estimate November 2021 and November 2025 DTGW values.

This approach assumes that the seasonal groundwater-level change observed between March and November 2012 is representative of seasonal variations in 2021 and 2025. While this introduces uncertainty, it provides a practical means of approximating DTGW during time periods that coincide with geophysical data acquisition.

An exception to the seasonal correction method described above was required for the northern portion of the study area, where monitoring wells with both March and November measurements were limited. This hindered the ability to apply the 2012 seasonal difference approach for estimating November 2021 and November 2025 DTGW in this region. In addition, the northeast corner of the study area was already weakly constrained in the cokriging interpolation due to the limited spatial distribution of November 2012 shallow monitoring wells. As a result, accurately representing DTGW in this region was critical to ensure that the water table was well-defined across the entire study area, including regions coinciding with geophysical data coverage.

The northernmost shallow monitoring well in the study area, (C-31-7)31acc-1, was of particular interest here. However, this well does not have measurements from 2012 and therefore could not be directly incorporated into the previously described seasonal difference workflow.

To address this limitation, a localized seasonal correction was estimated using inverse distance weighting (IDW). Four nearby monitoring wells with sufficient data in paired March and November measurements from the same year, were identified. For each of these nearby wells, the March to November DTGW difference was calculated. Where multiple years of data were available, differences were averaged to obtain a representative seasonal shift.

The seasonal correction for the northern well was then calculated as an inverse distance weighted average of these seasonal differences using a power parameter of 1 (Eq. (4)).

$$Seasonal\ Correction = \sum_{i=1}^{n} Difference_i \times \frac{1/D_i}{\sum(1/D_i)} \tag{4}$$

Here, D_i is the distance between the northernmost shallow monitoring well, (C-31-7)31acc-1, and nearby monitoring well i, with four neighboring wells included in the calculation. This approach assigns greater influence to closer wells while incorporating information from multiple surrounding observations.

Of the four nearby wells used in the inverse distance weighting calculation, two were classified as shallow wells, one was classified as a medium well, and one did not report a well depth. Although inclusion of the medium-depth and unknown-depth wells is not fully consistent with the earlier decision to restrict interpolation of the water table to shallow wells, this was considered a reasonable exception because of the limited monitoring well coverage in the northern portion of the study area. Furthermore, the inverse distance weighting calculation was used only to estimate a local seasonal correction for well (C-31-7)31acc-1 rather than to directly interpolate the final DTGW surface.

Using this method, a seasonal correction of 1.25 m was obtained and applied to March 2021 and March 2025 DTGW measurements to estimate corresponding November conditions for the northernmost shallow monitoring well, (C-31-7)31acc-1. The monitoring wells used in this inverse distance weighting procedure are shown in Figure 4, while Figure B1 in Appendix B provides the complete set of calculations.

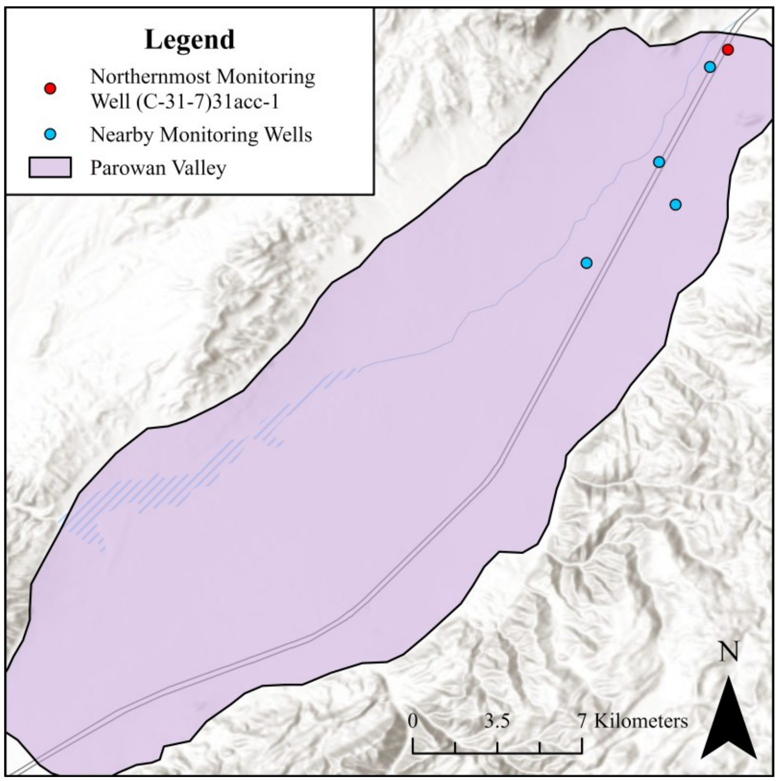

Figure 4: Northernmost and Nearby Monitoring Wells

With November 2021 and November 2025 DTGW values estimated for shallow monitoring wells, the next step was to quantify the difference between these estimates and the corresponding values from the November 2012 DTGW cokriging surface. These interannual differences were then interpolated across the study area using ordinary kriging with a linear variogram model to generate continuous interannual difference surfaces (Figure 5). The high values in the northeast corner of the study area are likely due to the lack of any monitoring wells with November 2012 measurements, which led to extrapolation of DTGW in that region during the cokriging process. The interpolated difference surfaces represent the spatially varying change in DTGW between November 2012 and the target years and were subsequently added to the November 2012 DTGW surface to generate final DTGW maps for November 2021 and November 2025, representing spatially continuous estimates of the water table corresponding to the geophysical data acquisition periods (Figure 5).

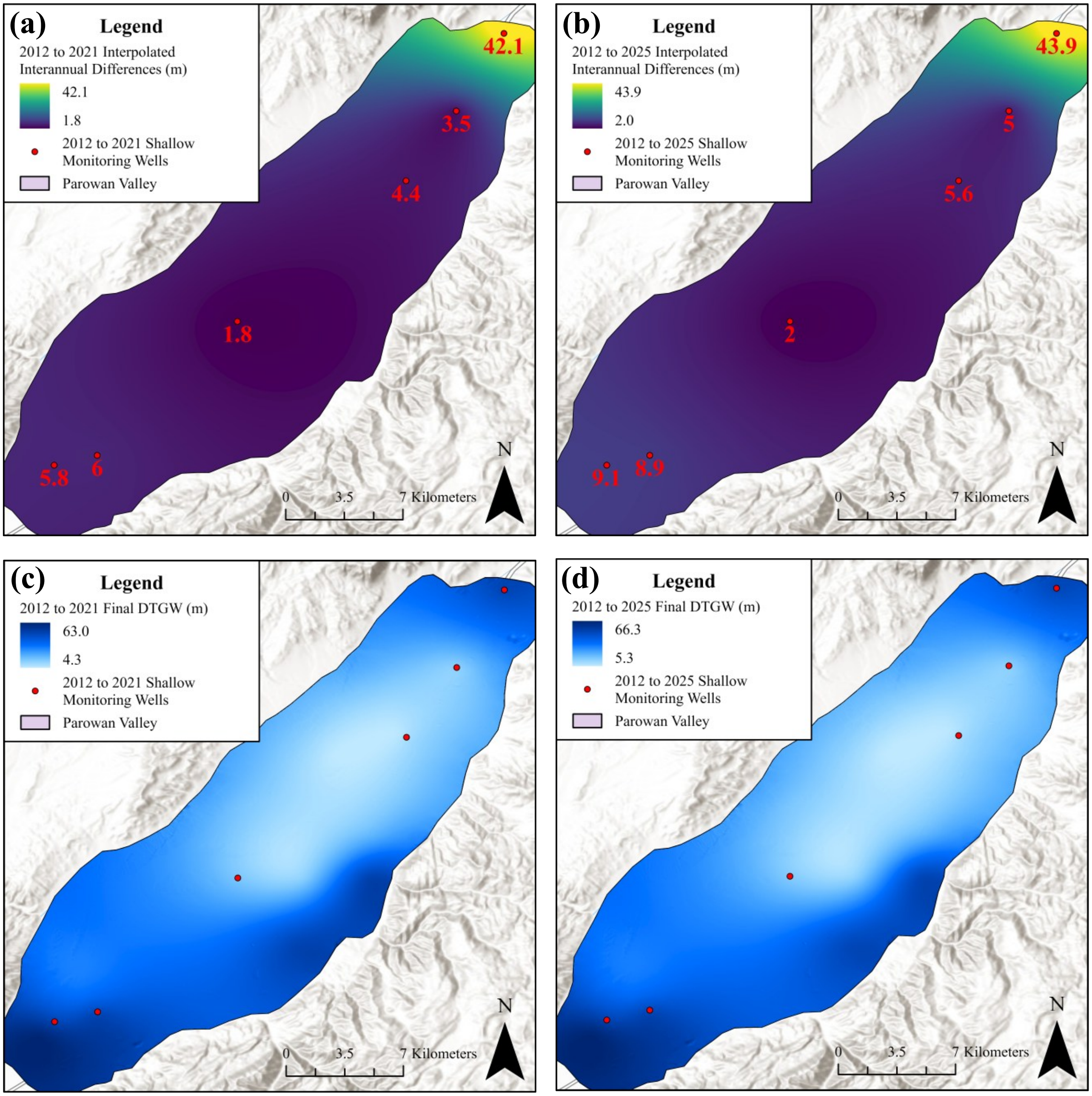

Figure 5: Interpolated Interannual Difference Surfaces and Resulting Final DTGW Surfaces. (a) 2012 to 2021 Interannual Differences. (b) 2012 to 2025 Interannual Differences. (c) Final November 2021 DTGW Surface. (d) Final November 2025 DTGW Surface.

These final DTGW surfaces provide the basis for delineating subsurface saturation conditions and enable direct integration with geophysical resistivity data. For the geophysical datasets, DTGW surfaces corresponding to the time of data acquisition were used to best represent saturation conditions during collection of the tTEM and WalkTEM measurements.

Unlike geophysical resistivity measurements, which are sensitive to time-dependent groundwater conditions, lithologic descriptions from drillers' logs represent relatively static subsurface material properties that do not change over time. However, classification of lithologic intervals as saturated or unsaturated remains dependent on water table position. Therefore, a single representative DTGW surface was required to consistently partition the lithologic dataset into saturated and unsaturated intervals across the study area. An average DTGW surface was created using the final November 2021 and November 2025 DTGW rasters and was used to consistently classify lithologic intervals across all rock physics transform error matrix runs (Figure 6).

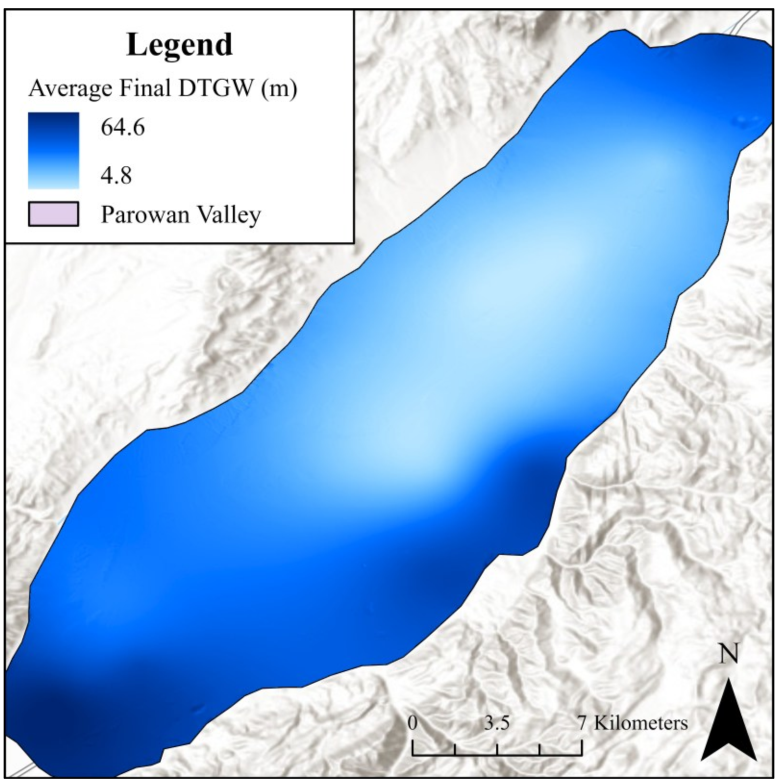

Figure 6: Average Final DTGW

The difference between the November 2021 and November 2025 DTGW surfaces was relatively small, with a maximum difference of 3.4 m as seen in Figure A5 in Appendix A. To evaluate whether this difference was significant for classification of saturated and unsaturated intervals, it was compared to the vertical discretization of both the lithologic and geophysical datasets used in this study.

For the drillers' log dataset, the average reported lithologic interval thickness across 194 logs was 12.2 m as seen in Figure B2 in Appendix B. This is substantially greater than the maximum difference between the 2021 and 2025 DTGW surfaces. Therefore, use of an average DTGW surface was considered a reasonable approximation for assigning lithologic intervals as saturated or unsaturated. Because lithologic descriptions represent relatively static subsurface material properties rather than time-dependent hydrologic observations, a single representative DTGW surface was sufficient for partitioning the drillers' logs into saturated and unsaturated intervals.

Using a common average DTGW surface for the lithologic dataset also ensured consistency between different runs of the rock physics transform error matrix. This avoided introducing bias that could result from selectively using either the 2021 or 2025 DTGW surface depending on which geophysical dataset was incorporated into a particular analysis. This consideration was especially important for the run integrating both tTEM and WalkTEM datasets, which correspond to November 2021 and November 2025 acquisition periods, respectively. In this case, use of a single temporally matched DTGW surface, from either 2021 or 2025, for the lithologic dataset would preferentially bias saturation classification toward one geophysical dataset over the other. Therefore, the average DTGW surface provided a consistent reference condition for lithologic classification across all model scenarios.

A similar comparison was performed for the geophysical datasets. Only geophysical layers intersecting the range of observed DTGW values (4.3 - 66.3 m) were considered, as these layers control classification of subsurface conditions as saturated or unsaturated. Within this depth range, the tTEM dataset had an average layer thickness of 3.2 m, while the WalkTEM dataset had an average layer thickness of 6.0 m, with calculations provided in Figure B3 in Appendix B. A point-by-point comparison with values extracted from the 2021 and 2025 DTGW differences surface showed that geophysical layer thicknesses exceeded the local DTGW differences at all sounding locations. Therefore, the observed differences between the November 2021 and November 2025 DTGW surfaces were smaller than the effective vertical resolution of the geophysical datasets at depths relevant to water table classification.

To summarize, DTGW surfaces corresponding to the geophysical data acquisition periods were retained for the tTEM and WalkTEM datasets to preserve temporal consistency between groundwater conditions and measured resistivity responses. Although the differences between the November 2021 and November 2025 DTGW surfaces were smaller than the effective vertical resolution of both geophysical datasets, use of temporally matched DTGW surfaces ensures that saturation classifications are referenced to groundwater conditions present during data acquisition. In contrast, the average DTGW surface was used for the drillers' log dataset because lithologic intervals are substantially thicker than the observed DTGW differences and because a single reference condition was required for consistent comparison across model scenarios. Together, these decisions provide a consistent framework for integrating datasets collected at different times while maintaining appropriate representation of groundwater conditions for each data type.

Overall, this workflow produced temporally constrained DTGW surfaces for integration with geophysical resistivity datasets while also establishing a consistent representative groundwater surface for lithologic classification. The combination of cokriging, seasonal corrections, and spatially interpolated interannual differences allowed groundwater conditions to be estimated throughout the study area despite limited monitoring well coverage and varying acquisition dates between datasets. This approach provided a practical framework for representing groundwater conditions at the time of geophysical data acquisition while maintaining a consistent reference condition for lithologic classification, thereby supporting subsequent rock physics transform analyses and comparisons across model scenarios.

2.3.4 Geophysical Data Processing

An ABEM WalkTEM 2 system was used for data acquisition, consisting of a 40 m × 40 m transmitter loop, a 10 m × 10 m RC-200 receiver coil, and a 59 cm × 59 cm RC-5 receiver coil (Figure 7). The WalkTEM system is a multi-channel transient electromagnetic (TEM) instrument employing dual-moment acquisition, allowing measurement of both low moment (LM) and high moment (HM) responses. The low moment provides improved resolution of the shallow subsurface, while the high moment enables increased depth of investigation.

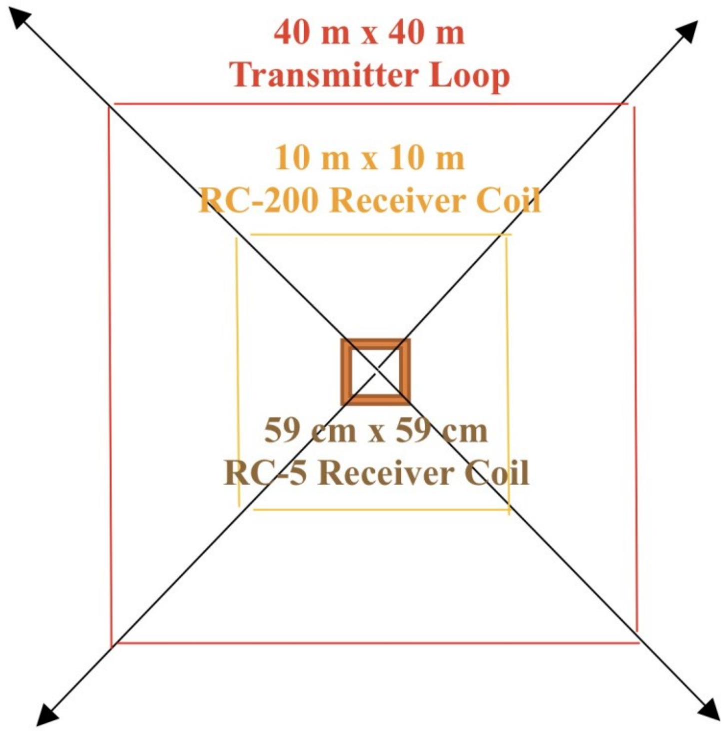

Figure 7: ABEM WalkTEM 2 System

Prior to the field campaign, survey locations were selected to minimize electromagnetic noise, with acquisition sites located at least 100 m from residential power lines and 200 m from major industrial infrastructure, following recommendations from geophysical researchers. These distances are consistent with, although slightly more conservative than, those recommended for ground-based TEM surveys by Maurya et al. (2020). This was necessary because overhead power lines are a significant source of noise in TEM measurements due to induced electromagnetic interference (Kirsch, 2009).

During the five-day field campaign, some planned locations were adjusted due to accessibility constraints, including private land access and dense vegetation such as sagebrush, which limited the ability to position the transmitter loop and receiver coils in ideal square configurations. At each site, a minimum of two repeat soundings were acquired to ensure data quality. These repeat measurements allowed for evaluation of noise conditions and selection of the highest-quality dataset for subsequent processing. Additionally, preliminary inversions were conducted in the field to verify data quality before proceeding to the next location.

Following field acquisition of the 33 WalkTEM soundings, data processing and inversion were performed using Aarhus SPIA. The first processing step involved removal of all gates falling below the estimated noise floor. These gates were identified by comparison of measured signal amplitudes to late-time noise responses and were excluded from subsequent inversion steps.

Following removal of below-noise gates, manual cleaning of the four WalkTEM channels was performed. Channels 1 and 2 correspond to the 59 cm × 59 cm RC-5 receiver coil, which provides improved sensitivity to shallow subsurface features. Channels 3 and 4 correspond to the 10 m × 10 m RC-200 receiver coil, which provides increased sensitivity to deeper subsurface features. Because the WalkTEM system employs dual-moment acquisition, channels 1 and 3 represent low moment measurements while channels 2 and 4 represent high moment measurements. Low moment data provides improved near-surface resolution, while high moment data increases depth of investigation.

Each channel exhibited characteristic noise behavior requiring channel-specific gate editing (Table 1). Early time gates from the RC-200 channels were commonly removed due to transmitter turn-off effects and near-field coupling, whereas late time gates from the RC-5 channels were frequently excluded because of reduced signal-to-noise ratios at depth. The objective of this gate editing process was to produce a continuous transient decay curve composed of the most reliable gates from each channel (Figure 8).

Table 1: Channel-Specific Gate Editing

Channel	Moment	Receiver Coil	Characteristics	Gate Editing
1	Low Moment	59 cm × 59 cm RC-5	Shallowest penetration so early gates are reliable	Keep early gates
			Noisy at late gates	Remove late gates
2	High Moment	59 cm × 59 cm RC-5	First few early gates are often distorted by turn-off waveform and coupling	Remove the first few early gate points
			Noisy at late gates	Remove late gates
3	Low Moment	10 m × 10 m RC-200	Large loop produces noise at early gates	Remove early gates
			Late gates are reliable	Keep late time gates but give preference to high moment RC-200
4	High Moment	10 m × 10 m RC-200	Large loop produces noise at early gates	Remove early gates
			Deepest penetration so late gates are reliable	Keep late time gates

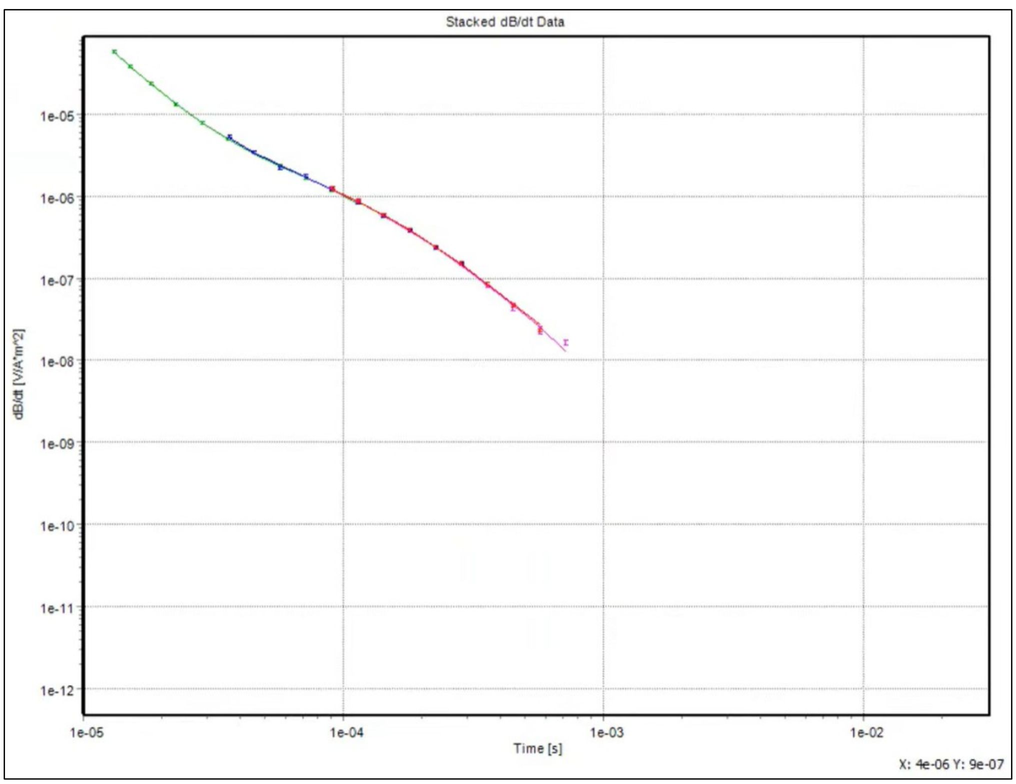

Figure 8: Transient Decay Curve from Channel-Specific Gate Editing (Guideline Geo, 2022)

Following manual data cleaning, smooth, 20-layer inversions were performed in SPIA for each sounding. Preferred inversion models were initially selected based on having the lowest data residual. In cases where multiple soundings at the same location produced nearly identical residuals, the model with the greater depth of investigation was selected. In all cases, visual inspection of the resistivity-depth structure was performed to ensure geological plausibility.

SPIA reports a dimensionless data residual that quantifies the agreement between observed and modeled transient electromagnetic responses. This data residual is calculated with Eq. (5) where d_{obs} is the observed data, d_{fwd} is the forward data, σ_d is the error in the observed data, and N is the number of data points (Auken et al., 2018).

$$d = \sqrt{\frac{1}{N}\sum_{i=1}^{N}\frac{\left(\log\left(d_{obs,i}\right) - \log\left(d_{fwd,i}\right)\right)^2}{\sigma_{d,i}^2}} \tag{5}$$

According to SPIA documentation, a residual value of 1 corresponds to a fit at the level of the data standard deviation for a sounding, while residual values below 1 indicate that modeled responses fit within the estimated standard deviation of the measured data (Aarhus GeoSoftware, n.d.). Although residuals greater than 1 may still be acceptable depending on site conditions and inversion objectives, soundings with residuals greater than 2 were excluded from further analysis because they exhibited comparatively poor inversion fits and reduced confidence in model reliability. This threshold was selected based on consultation with geophysical researchers and to maintain consistency with quality-control criteria applied to the Little Salt Lake tTEM dataset. Application of this criterion resulted in the exclusion of five WalkTEM soundings, leaving 28 usable soundings for subsequent analysis (Figure 9).

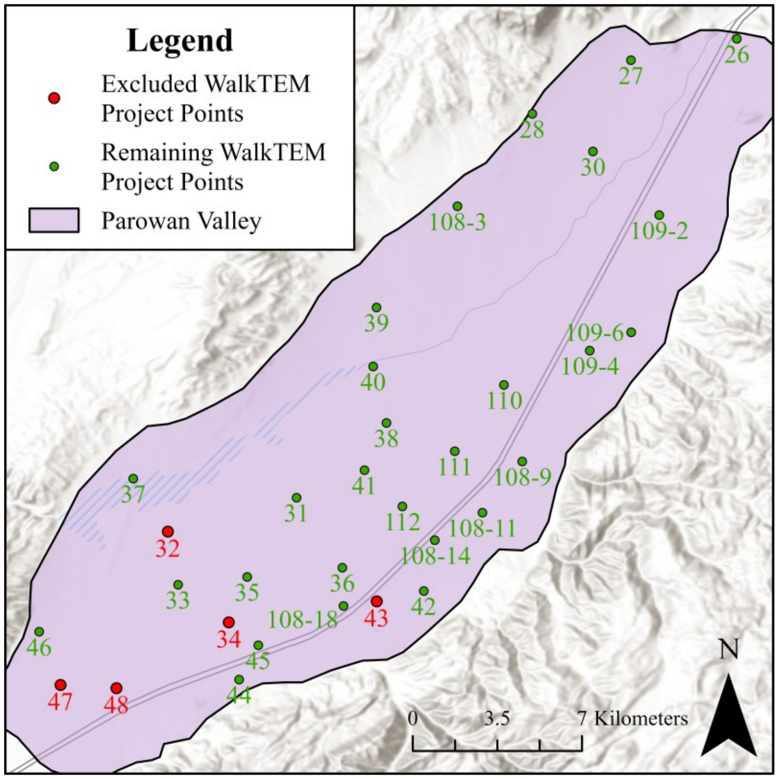

Figure 9: Excluded and Remaining WalkTEM Project Points

Field notes from excluded WalkTEM project points indicate several potential contributors to elevated residuals, including wet ground conditions from rainfall, difficulty maintaining proper loop geometry in dense vegetation, nearby infrastructure, and possible cable-related noise as seen in Table C1 in Appendix C. These factors may introduce coupling effects, increased noise, or other unmodeled responses that reduce inversion reliability.

With an acquisition date of November 2021, processing of the tTEM dataset had been completed prior to the start of this study. The exception was the Little Salt Lake portion, which was processed by the HydroGeophysics Group at Aarhus University in April 2026. For this dataset, tTEM soundings with data residuals greater than 2 were excluded to maintain consistency with the WalkTEM quality-control criteria.

In this clay-rich region, induced polarization (IP) effects were identified as a likely contributor to elevated residuals. Induced polarization occurs when subsurface materials temporarily store electrical charge and release it gradually following transmitter turn-off, producing an additional time-dependent response that is not fully represented in standard time-domain EM forward models.

Of particular interest were locations where the tTEM and WalkTEM datasets spatially overlapped. Although no soundings occupied the exact same location, seven pairs of tTEM and WalkTEM soundings located within 100 m of one another were identified (Figure 10). Comparative plots for these nearby soundings are provided in Table A1 in Appendix A. WalkTEM Project 34, while excluded from further analysis due to elevated residuals, is still included in these comparisons for reference purposes.

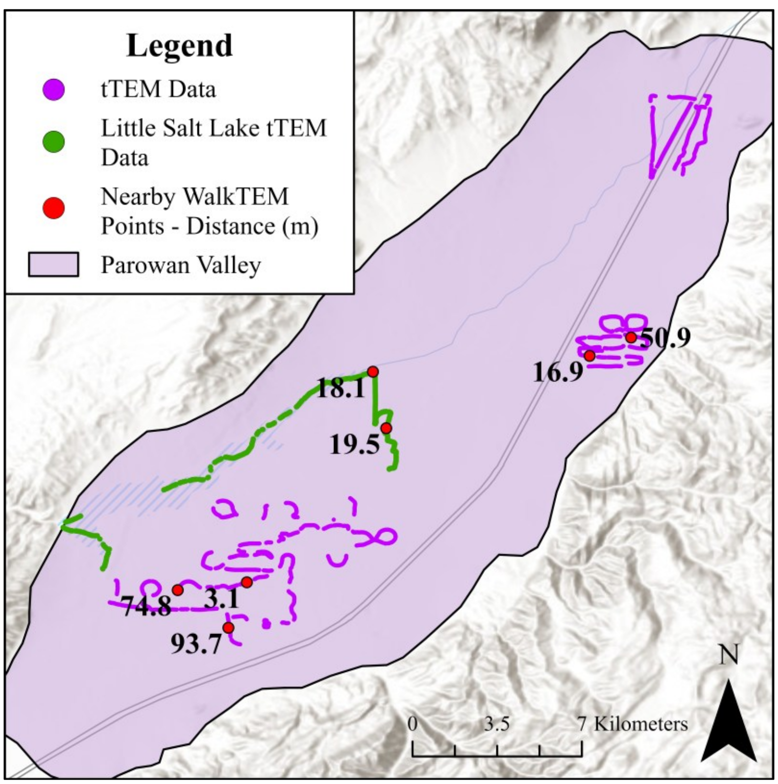

Figure 10: Nearby WalkTEM Points with Distances to tTEM Data

Comparing the tTEM and WalkTEM inversion results, the closest agreements occur at WalkTEM Projects 38, 40, and 109-6. In contrast, WalkTEM Projects 33, 34, 35, and 109-4 exhibit more distinct differences between the two datasets. One possible explanation for these differences is the approximately four-year gap between acquisition dates. Figure A5 in Appendix A shows a decline in the water table during this period which could increase the thickness of the unsaturated zone and produce higher resistivity values in the more recent WalkTEM dataset.

This interpretation is supported by the observation that the closest agreements between tTEM and WalkTEM inversions occur in regions where water table decline was relatively minor, whereas the largest differences tend to occur in regions that experienced greater water table decline. WalkTEM Project 109-4 represents an exception, as distinct differences between the tTEM and WalkTEM inversions are still observed despite relatively limited water table decline in that area. It should also be recognized that geophysical inversions are inherently nonunique, and the datasets were processed independently by different analysts, both of which may contribute to differences between nearby soundings.

2.4 Modeling Approach

2.4.1 Depth of Investigation

A depth of investigation (DOI) of 50 m was applied to the tTEM dataset. The exception to this was the Little Salt Lake portion, where the "Standard DOI" reported by the inversion software was used instead of a constant 50 m threshold. This adjustment was made because the Little Salt Lake region is characterized by clay-rich deposits that may produce induced polarization (IP) effects, potentially reducing DOI estimates in portions of the dataset. Restricting interpretation to the inversion-derived DOI values helped minimize the inclusion of less reliable subsurface information. In contrast, a DOI of 100 m was used for the WalkTEM dataset due to the system's greater depth sensitivity and ability to image deeper subsurface conditions relative to the tTEM system.

For the drillers' log dataset, the DOI varied depending on the model scenario. For rock physics transform error matrix runs that did not incorporate WalkTEM data, a drillers' log DOI of 50 m was used to maintain consistency with the tTEM dataset. In contrast, the run incorporating WalkTEM data utilized a drillers' log DOI of 100 m to align with the greater investigation depth of the WalkTEM system. Extending the drillers' log DOI ensured that both lithologic and geophysical datasets characterized comparable subsurface intervals while also incorporating deeper portions of the saturated zone that may not be adequately represented within the upper 50 m.

2.4.2 Saturated vs. Unsaturated Zone Delineation

The geophysical and lithologic datasets were separated into saturated and unsaturated zones using the interpolated DTGW surfaces, as electrical resistivity is strongly influenced by subsurface saturation conditions. The lithologic dataset, composed of drillers' logs, referenced the average DTGW surface (Figure 6), while the geophysical datasets referenced the DTGW surfaces corresponding to their respective acquisition dates of November 2021 for the tTEM dataset and November 2025 for the WalkTEM dataset (Figure 5).

For depth intervals intersecting the interpolated water level, layer thicknesses were proportionally divided between the saturated and unsaturated zones based on the portion of the interval located above and below the DTGW surface. This approach helped minimize misclassification of partially saturated layers during subsequent analysis.

2.4.3 Rock Physics Transform

Because electrical resistivity is influenced by factors such as grain size, saturation, and clay content, resistivity measurements can be used as a proxy for lithology in subsurface classification. This allows for geophysical datasets, which report resistivity, to be converted to lithologic classifications using a rock physics transform. A primary challenge of this approach is determining representative resistivity thresholds associated with different lithologic units.

Following lithologic classification, lithology weighted averages were calculated for the saturated and unsaturated zones at each data point for both the geophysical and lithologic datasets. Numerical values were assigned to the three lithologic description categories defined from the drillers' logs, where coarse-grained materials were assigned a value of 1, mixed-grained materials a value of 0.5, and fine-grained materials a value of 0 (Table 2). As a result, interpolated outputs are expressed as fractions of coarse-grained material within the subsurface. An example lithology weighted average calculation is provided in Figure B4 in Appendix B.

Table 2: Lithology Classification Values

Lithology Classification	Value
Coarse-Grained	1
Mixed-Grained	0.5
Fine-Grained	0

2.4.4 Error Matrix Approach

Ranges of resistivity thresholds for saturated and unsaturated coarse-grained and fine-grained materials were evaluated through an iterative optimization framework to identify representative values for the rock physics transform. Published resistivity values were referenced to define these ranges to encompass all plausible parameter combinations and provide a comprehensive evaluation (Li et al., 2024). The ranges used in the rock physics transform error matrix for this study are provided in Table 3. An exponential spacing function was used instead of equal linear intervals to provide greater sampling density at lower resistivity values, where lithologic classifications may be more sensitive to small changes in resistivity. Additionally, 20 values within each resistivity range were evaluated within the rock physics transform error matrix.

Table 3: Resistivity Threshold Ranges for Rock Physics Transform Error Matrix

Saturated Zone		**Unsaturated Zone**	
Coarse-Grained	Fine-Grained	Coarse-Grained	Fine-Grained
15 Ω·m - 65 Ω·m	1 Ω·m - 30 Ω·m	25 Ω·m - 75 Ω·m	10 Ω·m - 40 Ω·m

To prevent unrealistic or nonphysical classification scenarios during optimization, gap and fraction constraints were implemented within the rock physics transform error matrix framework. One potential issue occurs when optimization converges toward nearly identical resistivity thresholds for coarse-grained and fine-grained materials, minimizing the interval assigned to mixed-grained material lithology. To prevent this outcome, a minimum gap between coarse-grained and fine-grained material resistivities was enforced (Table 4).

A second potential issue occurs when optimization converges toward unrealistically large mixed-grained material lithology intervals in order to artificially reduce root mean square error (RMSE). Because RMSE penalizes large deviations, overly smooth models may appear favorable despite producing unrealistic lithologic distributions. Minimum coarse-grained and fine-grained material fractions along with a maximum mixed-grained material fraction were therefore implemented to maintain physically reasonable lithologic proportions during optimization (Table 4).

Table 4: Gap and Fraction Constraints

Parameter	Value	Purpose
Minimum Gap between Coarse-Grained and Fine-Grained Material Resistivities	0.1	Prevent convergence toward nearly identical coarse-grained and fine-grained material resistivity thresholds
Minimum Coarse-Grained Material Fraction	0.1	Prevent an unrealistically large mixed-grained material lithology interval
Minimum Fine-Grained Material Fraction	0.1	
Maximum Mixed-Grained Material Fraction	0.7	

Scenarios satisfying the gap and fraction constraints specified in Table 4 were evaluated within the rock physics transform error matrix, while scenarios failing to satisfy these constraints were excluded. Optimization involved iteratively evaluating all specified combinations of saturated and unsaturated coarse-grained and fine-grained material resistivity thresholds and reporting the resulting model performance metrics.

2.4.5 Interpolation

Because geophysical and lithologic observations are only available at discrete locations throughout the study area, geostatistical interpolation was required to estimate the spatial distribution of subsurface lithology between measurement locations. Ordinary kriging with a spherical variogram model was utilized to interpolate the fraction of coarse-grained material within the saturated and unsaturated zones separately.

For each set of resistivity thresholds tested in the optimization matrix, lithologic classifications were generated for the available geophysical datasets, and interpolation was performed using those data in combination with a training subset of the drillers' log dataset while excluding a held-out validation dataset for model evaluation.

2.4.6 Model Evaluation

To evaluate model performance, approximately 25% of the drillers' logs were withheld from the interpolation workflow and reserved for independent validation. Rather than selecting validation logs using a purely random sampling approach, k-means clustering was applied to the drillers' log UTMX and UTMY spatial coordinates to ensure that held-out logs were distributed throughout the study area and adequately represented spatial variability.

The total number of clusters was set equal to the desired number of held-out drillers' logs. A single log was then randomly selected from each cluster to create the validation dataset, resulting in a spatially balanced subset of 48 held-out drillers' logs. The remaining logs were retained as the training dataset used during interpolation (Figure 11).

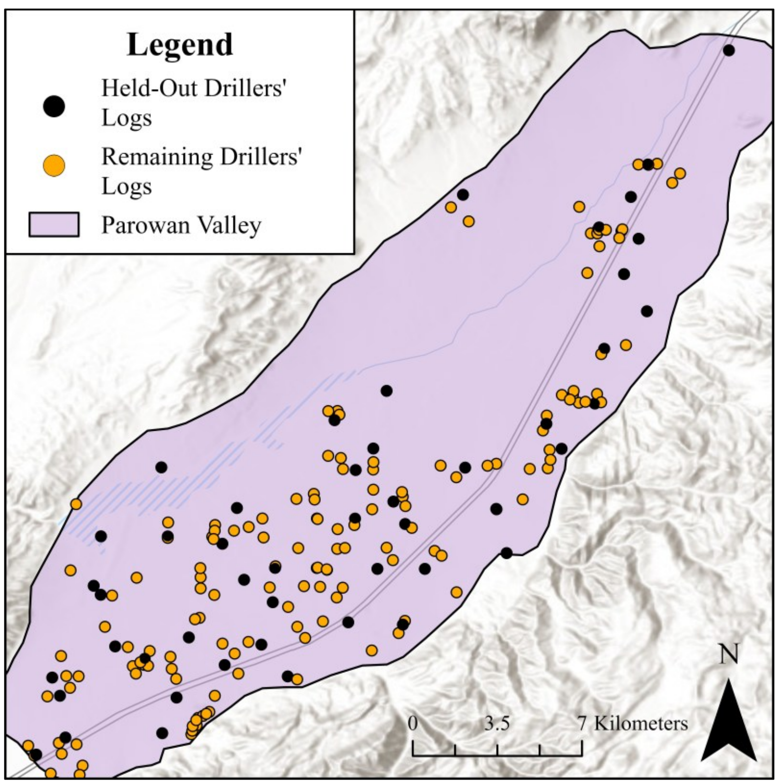

Figure 11: Held-Out and Remaining Drillers' Logs

Model performance was evaluated by comparing interpolated lithology values at held-out drillers' log locations against observed lithology values derived from drillers' logs. Root mean square error (RMSE) and Kling-Gupta efficiency (KGE) were the selected performance metrics for this study.

RMSE quantifies the error between interpolated and observed values, with lower values indicating better model performance. RMSE is calculated with Eq. (6), where $\hat{y}_i$ represents the interpolated lithology value, y_i represents the observed lithology value, and n represents the total number of observations.

$$RMSE = \sqrt{\frac{1}{n}\sum_{i=1}^{n}(\hat{y}_i - y_i)^2} \tag{6}$$

KGE evaluates model performance through three components: correlation (r), variability (α), and bias (β) (Eq. (7)). Variability is calculated as the ratio of the standard deviation of interpolated values to the standard deviation of observed values, while bias is calculated as the ratio of the mean of interpolated values to the mean of observed values. A KGE value of 1 represents a perfect agreement between interpolated and observed values, while values greater than -0.41 indicate model performance superior to simply using the mean of the observed values.

$$KGE = 1 - \sqrt{(r-1)^2 + (\alpha - 1)^2 + (\beta - 1)^2} \tag{7}$$

KGE was included because RMSE alone frequently favors overly smooth interpolation results. Because RMSE heavily penalizes large individual errors, interpolation scenarios with reduced spatial variability could produce artificially low RMSE values despite failing to represent realistic subsurface heterogeneity.

To address this limitation, KGE was incorporated alongside RMSE in model evaluation. Because KGE explicitly evaluates correlation, variability, and bias between interpolated and observed values, it provides additional sensitivity to overly smoothed interpolation results that may otherwise appear favorable when evaluated using RMSE alone.

With two performance metrics being utilized, a combined performance score was developed to allow for direct comparison between different runs of the rock physics transform error matrix. First, RMSE and KGE values were normalized independently using min-max normalization. This was done with Eq. (8), where x represents the original performance metric value, x_{min} represents the minimum observed value, and x_{max} represents the maximum observed value across all model runs.

$$x' = \frac{x - x_{min}}{x_{max} - x_{min}} \tag{8}$$

Because lower RMSE values indicate improved model performance whereas higher KGE values indicate improved model performance, normalized KGE values were inverted to maintain a consistent scoring convention where lower values are better (Eq. (9)).

$$Flipped\ KGE = 1 - KGE \tag{9}$$

The combined score was then calculated using Eq. (10), where greater weight was assigned to RMSE because minimizing interpolation error remained the primary objective of the study. However, KGE was also incorporated to ensure that interpolation scenarios reproduced realistic spatial variability and avoided overly smooth subsurface representations.

$$Combined\ Score = (0.7 \times RMSE) + (0.3 \times Flipped\ KGE) \tag{10}$$

The scenario producing the lowest combined score was selected as the optimal model for each saturated and unsaturated zone. This approach ensured that selected resistivity thresholds minimized interpolation error while also preserving the spatial heterogeneity expected within the study area.

2.5 Scenario Design

To evaluate whether integrating geophysical and lithologic datasets results in improved subsurface characterization relative to interpolation performed using lithologic observations alone, three separate rock physics transform error matrix runs were developed and compared. Each run utilized the same interpolation workflow, held-out validation dataset, optimization procedure, and model evaluation metrics, with only the input datasets varying between runs. This approach allowed the influence of dataset integration on interpolation performance and subsurface characterization to be isolated and evaluated.

Run #1, referred to as "Initial Results", utilized the tTEM and drillers' log datasets to establish a baseline integrated interpolation model. This run represents the primary workflow for combining geophysical and lithologic information within the study area.

Run #2, referred to as "Adding WalkTEM Data", followed the same methodology as Run #1 but incorporated an additional 28 WalkTEM soundings with data residuals less than 2. To maintain consistency with the greater investigation depth of the WalkTEM system, the drillers' log DOI was increased from 50 m to 100 m. The purpose of this run was to evaluate whether increasing both the spatial coverage of geophysical observations and the depth of lithologic information influenced interpolation performance and characterization of subsurface heterogeneity.

Run #3, referred to as "Drillers' Logs Only for Comparison", utilized only the lithologic dataset for interpolation with a 50 m DOI, excluding all geophysical observations. This run served as a reference case for comparison against the integrated interpolation workflows developed in Runs #1 and #2. A summary of the three rock physics transform error matrix runs is provided in Table 5.

Table 5: Rock Physics Transform Error Matrix Runs

Run	Geophysical Dataset	Lithologic Dataset	Purpose
Run #1 – Initial Results	tTEM (50 m DOI)	Drillers' Logs (50 m DOI)	Baseline integrated interpolation model
Run #2 – Adding WalkTEM Data	tTEM (50 m DOI) and WalkTEM (100 m DOI)	Drillers' Logs (100 m DOI)	Evaluate influence of added WalkTEM data and increased lithologic DOI
Run #3 – Drillers' Logs Only for Comparison	None	Drillers' Logs (50 m DOI)	Reference comparison against integrated models

3. RESULTS

3.1 Error Matrices

Error matrices were created for Runs #1 and #2 to evaluate how model performance varied across the tested resistivity threshold combinations. Since Run #3 does not utilize geophysical data and therefore does not require optimization of resistivity thresholds, this run does not have associated error matrices. The error matrices shown in Figure 12 display all tested resistivity threshold combinations. For scenarios that satisfy the gap and fraction constraints, a combined score is reported, where green indicates stronger model performance and red indicates weaker model performance. The optimal model, corresponding to the lowest combined score, is outlined in blue. Scenarios that did not satisfy the selection criteria are represented by greyed-out cells labeled according to the reason for exclusion (Table 6). All exclusion reasons correspond to the gap and fraction constraints discussed previously, with the exception of the scenario where the fine-grained material resistivity exceeds the coarse-grained material resistivity as this is inconsistent with observed electrical resistivity relationships (Olabode & San, 2023).

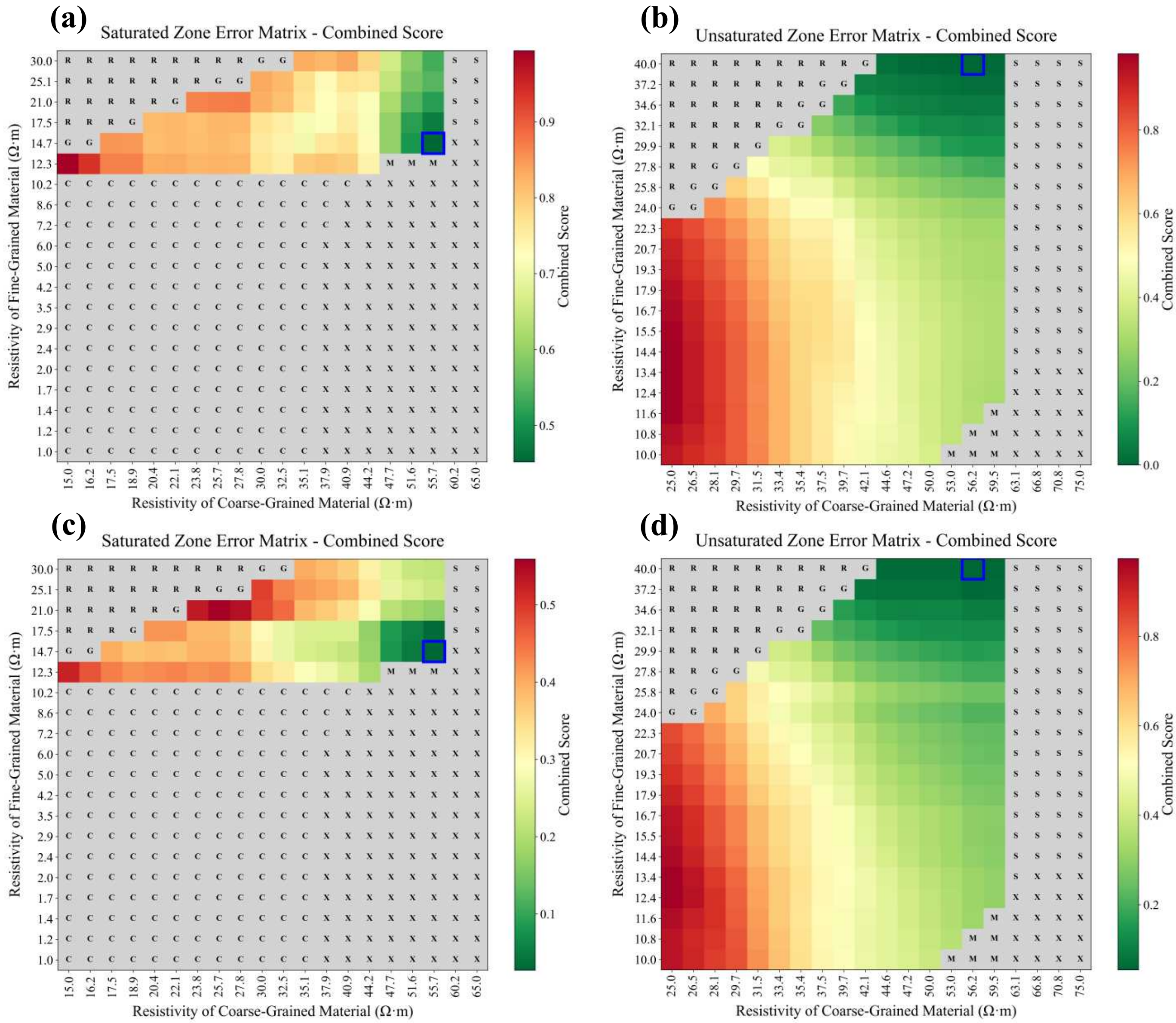

Figure 12: Combined Score Error Matrices. (a) Run #1 Saturated Zone. (b) Run #1 Unsaturated Zone. (c) Run #2 Saturated Zone. (d) Run #2 Unsaturated Zone.

Table 6: Error Matrix Exclusion Reasons

Exclusion Reason	**Letter Code**
Failed Minimum Gap between Coarse-Grained and Fine-Grained Material Resistivities	G
Failed Minimum Coarse-Grained Material Fraction	S
Failed Minimum Fine-Grained Material Fraction	C
Failed Maximum Mixed-Grained Material Fraction	M
Fine-Grained Material Resistivity Exceeds Coarse-Grained Material Resistivity	R
Multiple Exclusion Reasons	X

For each optimal model, the representative resistivity thresholds for Runs #1 and #2, along with the performance metrics for all three runs, are summarized in Table 7. For each metric, values highlighted in green indicate the best performing run while values highlighted in red indicate the worst performing run. Several trends are observed across the optimal model results. First, optimal saturated zone resistivity thresholds are consistently lower than the corresponding unsaturated zone thresholds, which is consistent with the expected influence of groundwater saturation on resistivity (McCarter, 1984). Second, adding WalkTEM data and increasing the drillers' log DOI improved the saturated zone combined score relative to Run #1, but did not improve the unsaturated zone combined score. Finally, Run #3, which used only the drillers' log dataset with a 50 m DOI, produced the weakest overall performance in both the saturated and unsaturated zones, indicating improved interpolation performance when geophysical data were incorporated alongside lithologic observations.

Table 7: Rock Physics Transform Error Matrix Results

	Saturated Zone					**Unsaturated Zone**				
	Coarse-Grained Material	**Fine-Grained Material**	**RMSE**	**KGE**	**Combined Score**	**Coarse-Grained Material**	**Fine-Grained Material**	**RMSE**	**KGE**	**Combined Score**
Run #1 – Initial Results	> 55.7 Ω·m	< 14.7 Ω·m	0.323	0.184	0.452	> 56.2 Ω·m	< 40.0 Ω·m	0.246	0.454	0.000
Run #2 – Adding WalkTEM Data	> 55.7 Ω·m	< 14.7 Ω·m	0.266	0.290	0.027	> 56.2 Ω·m	< 40.0 Ω·m	0.255	0.454	0.054
Run #3 – Drillers' Logs Only for Comparison	N/A	N/A	0.321	0.115	0.526	N/A	N/A	0.247	0.205	0.248

3.2 Interpolated Fraction of Coarse-Grained Material Maps

Interpolated fraction of coarse-grained material maps were generated for the optimal model from each run for both the saturated and unsaturated zones. Held-out wells, mapped alluvial fan deposits, and the Little Salt Lake were overlaid on the interpolation surfaces to allow for visual comparison between interpolated lithology, observed lithology, and expected geomorphic settings. The same held-out well set was used across all three runs, except in the saturated zone of Run #2, where the increased DOI from 50 m to 100 m resulted in a different validation dataset.

The interpolated fraction of coarse-grained material maps for Runs #1 through #3 are shown in Figure 13. Agreement between interpolated and observed lithology varies spatially throughout the study area, with some held-out wells closely matching nearby interpolated values while others exhibit larger discrepancies. Visual comparison between Runs #1 and #2 reveals only minor differences in interpolation patterns, indicating that the quantitative performance metrics summarized in Table 7 provide a more effective basis for evaluating the influence of added WalkTEM data and an increased drillers' log DOI. In contrast to Runs #1 and #2, Run #3 exhibits smoother interpolation surfaces with reduced spatial variability, particularly within the saturated zone. Regions of lower coarse-grained material fractions in Runs #1 and #2 generally correspond more closely with the Little Salt Lake, while regions of higher coarse-grained material fractions align more consistently with mapped alluvial fan deposits. The observed versus interpolated lithology plots found in Figure A6 in Appendix A further support this interpretation. Compared with Runs #1 and #2, Run #3 exhibits a noticeably narrower range of interpolated lithology values, indicating a reduced ability to reproduce the full range of observed lithologic variability when only drillers' logs are used for interpolation.

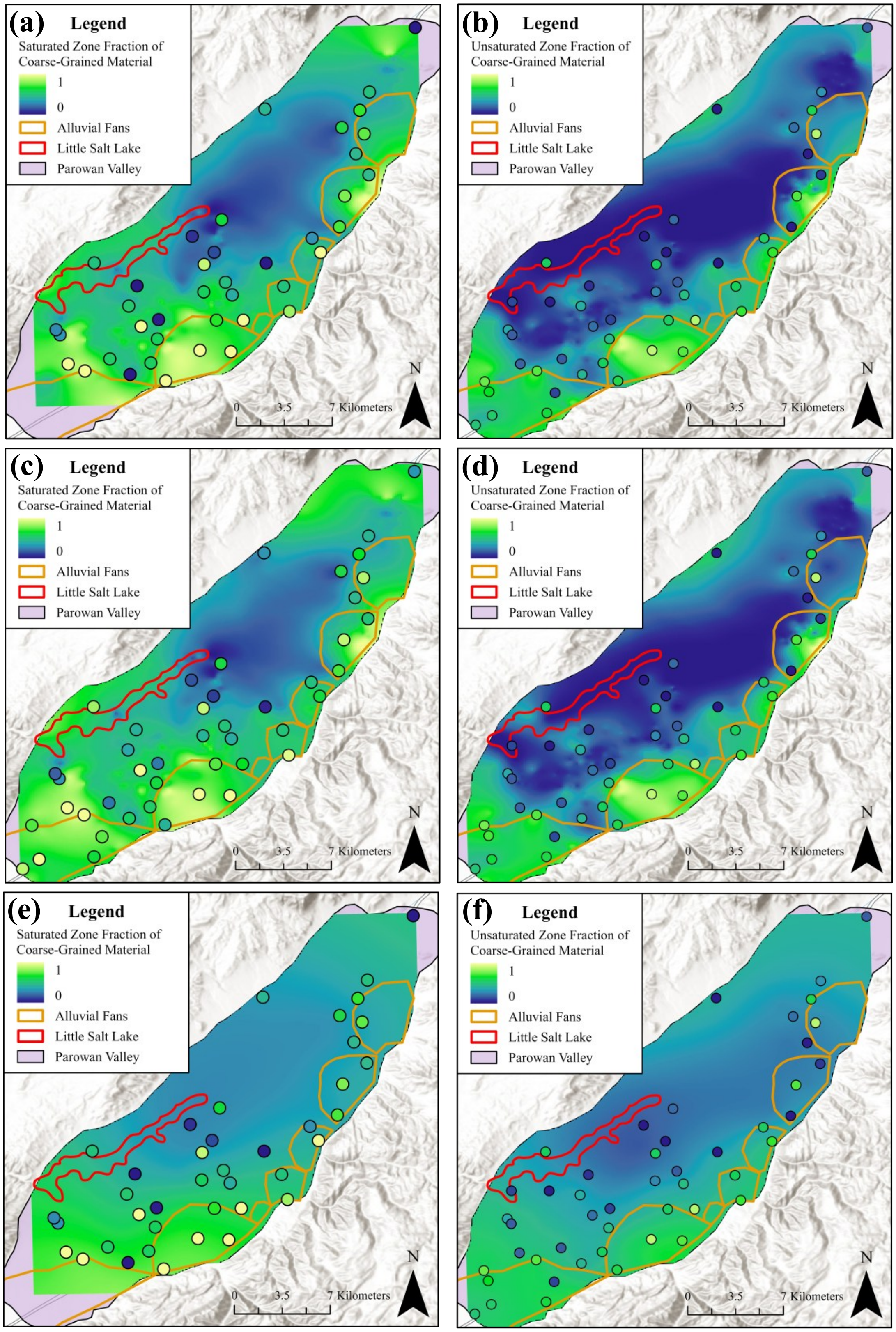

Figure 13: Interpolated Fraction of Coarse-Grained Material Maps. (a) Run #1 Saturated Zone. (b) Run #1 Unsaturated Zone. (c) Run #2 Saturated Zone. (d) Run #2 Unsaturated Zone. (e) Run #3 Saturated Zone. (f) Run #3 Unsaturated Zone.

4. DISCUSSION

4.1 Integrated Approach

The primary objective of this study was to evaluate whether integrating geophysical and lithologic datasets improves subsurface characterization relative to interpolation performed using lithologic observations alone. Results from Run #3, which utilized only drillers' logs during interpolation, indicate weaker overall model performance compared to the integrated workflows developed in Runs #1 and #2. Although RMSE alone did not consistently identify the lithology-only approach as the worst performing run, inclusion of KGE within the combined score highlighted the importance of spatial variability in evaluating interpolation performance as Run #3 produced the highest combined scores in both the saturated and unsaturated zones. This suggests that incorporation of geophysical data contributed to more spatially representative interpolation surfaces, particularly in areas where lithologic observations alone provided limited spatial coverage.

Because ordinary kriging relies entirely on the spatial distribution of input observations, interpolation uncertainty increases in regions with sparse data coverage. Incorporation of geophysical data increases the spatial density of subsurface information, allowing lithologic estimates within these regions to be informed by a greater number of observations than would be possible using drillers' logs alone. This is particularly evident near the Little Salt Lake and within the northern and southern portions of Parowan Valley, where relatively few drillers' logs exist. Although these regions cannot be independently validated because of the limited availability of ground truth data, the integrated approach provides more spatially representative subsurface characterization while preserving heterogeneity that is less apparent when interpolation relies solely on the drillers' log dataset.

The improved performance observed in the integrated approach is likely related to the increased spatial density provided by geophysical observations relative to the drillers' log dataset alone. This is especially evident in the interpolation surfaces produced for Run #3, which exhibit noticeably smoother patterns and reduced spatial variability. In comparison, Runs #1 and #2 more closely align with expected geomorphic settings, including lower fractions of coarse-grained material within the Little Salt Lake region and higher fractions of coarse-grained material associated with mapped alluvial fan deposits. These results suggest that the addition of geophysical data helped preserve spatial heterogeneity that was not captured when interpolation relied solely on drillers' logs.

An additional insight is provided by comparison with the land subsidence rate map found in Figure A7 in Appendix A. Negative values indicate greater land subsidence and are concentrated in the southwestern portion of the study area adjacent to the Little Salt Lake. This region corresponds closely with lower fractions of coarse-grained material in the interpolated lithology maps for Runs #1 and #2, particularly within the unsaturated zone. This spatial agreement provides support from an independent dataset for the integrated interpolation approach, as areas experiencing greater land subsidence coincide with fine-grained deposits that are more susceptible to compaction.

Despite the benefits of adding geophysical data, drillers' logs remain an important component of the interpolation workflow because they provide direct lithologic observations and therefore do not require optimization of resistivity thresholds. In contrast, geophysical data requires indirect lithologic classification through the rock physics transform, introducing uncertainty associated with threshold selection and inversion results. For this reason, integration of the two datasets reduces ambiguity by combining direct lithologic observations with the improved spatial coverage provided by geophysical data. An additional advantage of the proposed interpolation framework is that geophysical and lithologic data do not need to be co-located. Unlike many previous studies, where lithologic observations are primarily used to constrain, calibrate, interpret, or validate nearby geophysical measurements, the integrated interpolation approach retains both datasets as active inputs to the final interpolation surface. Consequently, geophysical surveys can extend subsurface characterization into regions where drillers' logs are sparse or absent, reducing the need for dense lithologic observations throughout the survey area.

In addition to evaluating the integrated interpolation approach, comparison between Runs #1 and #2 provides insight into the influence of adding WalkTEM data coupled with an increased drillers' log DOI. This comparison reveals improved saturated zone performance but did not improve performance within the unsaturated zone. This finding is consistent with the greater depth of investigation associated with the WalkTEM system relative to the tTEM system. Because the saturated zone occurs deeper within the subsurface, the additional depth penetration provided by WalkTEM data likely contributed lithologic information relevant to saturated zone interpolation. However, the increased drillers' log DOI used in Run #2 is also likely a contributing factor to the improved saturated zone performance. Consequently, the observed improvements cannot be attributed solely to the addition of WalkTEM data. In contrast, the unsaturated zone is comparatively shallow and was already well represented by the existing tTEM dataset, limiting the added benefit of the 28 additional WalkTEM soundings.

4.2 Limitations

One limitation of this study involves gaps in spatial data coverage throughout the study area. WalkTEM data acquisition was initially planned for regions with sparse tTEM coverage and limited drillers' log data. However, adjustments in the field were required because of accessibility constraints related to private land access and dense vegetation, particularly sagebrush. As a result, some portions of the study area remained underrepresented within the integrated dataset, forcing interpolation within these regions to rely more heavily on distant neighboring data points. This potentially resulted in over smoothing of local variability, therefore reducing the ability to resolve smaller scale subsurface heterogeneity. This limitation highlights the importance of considering geophysical data acquisition systems that are better suited for navigating difficult terrain in future investigations.

Another limitation of this study relates to the monitoring wells used to estimate depth to groundwater. Limiting the analysis to shallow wells to avoid confined aquifer conditions reduced the number of usable wells and resulted in poorer spatial coverage across the study area. Consequently, reduced monitoring well coverage likely limited the accuracy of DTGW surface interpolation, influencing zonal classifications and associated lithologic interpretation results.

A final limitation of this study is that degree of saturation was treated as the primary factor influencing electrical resistivity during lithologic classification. Although groundwater saturation strongly affects resistivity, other factors such as salinity can also significantly influence geophysical responses (Knight et al., 2018). This is particularly relevant near the Little Salt Lake, where elevated salinity may alter resistivity independent of lithology. As a result, some resistivity variations within the study area may reflect hydrochemical conditions rather than lithologic differences alone.

4.3 Sources of Uncertainty

Moving to sources of uncertainty within this study, the gap and fraction constraint values were applied consistently across the entire study area. However, subsurface heterogeneity suggests that different constraint values may be more appropriate in certain regions. For example, the Little Salt Lake region is expected to contain a greater proportion of fine-grained material, suggesting that lower fractions of coarse-grained material may be conceptually reasonable in this area. As a result, applying uniform constraint values across the study area introduces uncertainty into the rock physics transform error matrix.

Another source of uncertainty relates to the inversions performed for the tTEM and WalkTEM datasets. These inversions were completed independently and by different individuals, and because geophysical inversion is inherently nonunique, multiple subsurface models may reasonably explain the observed data. Consequently, uncertainty is associated with the resulting geophysical datasets, particularly for Run #2 where tTEM and WalkTEM datasets were used together.

A final source of uncertainty in this study is the use of an average DTGW surface for the drillers' log dataset. Because the drillers' logs were collected over a wide range of acquisition dates, an average between the November 2021 and November 2025 DTGW surfaces was determined to be the most reasonable approach. However, this creates a scenario where nearby geophysical and lithologic observations may reference different groundwater conditions, introducing temporal inconsistency into saturated and unsaturated zone classifications and therefore increasing uncertainty in subsurface lithologic characterization.

4.4 Implications Beyond Study Area

In applying this study's methodology to other study areas, it is beneficial to incorporate existing geomorphic knowledge when ground truth data are limited. Within the Parowan Valley study area, geomorphic context was provided by mapped alluvial fan deposits and the Little Salt Lake region. These geomorphic features served as an additional framework for evaluating interpolated fraction of coarse-grained material maps and interpreting inconsistencies within the drillers' log dataset. The absence of standardized reporting practices for drillers' logs in Utah results in inconsistencies in lithologic descriptions across logs. In some cases, drillers' logs located within mapped alluvial fan deposits reported relatively high fractions of fine-grained material, despite coarse-grained material being more conceptually consistent with this depositional environment. Without geomorphic context, these observations could be interpreted as major interpolation errors. However, incorporating geomorphic information provided additional confidence in identifying regions where inconsistencies may instead reflect variability in drillers' log reporting practices rather than interpolation performance alone.

Another implication beyond the Parowan Valley study area is that different geophysical data acquisition systems possess unique advantages and limitations depending on study objectives and field conditions. Selection of the most appropriate geophysical system should therefore consider factors such as study area size, accessibility, desired spatial coverage, and required depth of investigation. For example, the tTEM system allows for rapid data acquisition across large study areas but requires relatively open terrain that can be traversed by vehicle. In contrast, the WalkTEM system provides greater flexibility in difficult terrain because data are collected at stationary locations. However, acquisition is significantly slower and therefore less efficient for large study areas. Depth of investigation is another important consideration, as the WalkTEM system can image deeper portions of the subsurface relative to the tTEM system.

5. CONCLUSION

This study introduced a novel approach for subsurface characterization through the integration of geophysical and lithologic datasets. Comparisons between the three rock physics transform error matrix runs demonstrated that the integrated interpolation approach outperformed interpolation using only drillers' logs. These results highlight the value of incorporating geophysical data into groundwater hydrology and management applications, particularly when combined with lithologic observations that provide direct subsurface information but may contain inconsistencies resulting from the absence of standardized reporting practices.

The results of this study can support groundwater management efforts within the Parowan Valley, particularly in addressing concerns related to land subsidence and groundwater availability. Beyond the Parowan Valley study area, this methodology may be applicable to other regions where subsurface characterization is of interest, but direct sampling methods are spatially limited because of cost or logistical constraints. In these settings, geophysical data can complement lithologic observations to improve interpolation performance and subsurface interpretation.

Future work could introduce a drillers' log scoring criteria to evaluate whether excluding lower quality logs improves interpolation performance. Additional analysis of monitoring wells and aquifer conditions could improve depth to groundwater estimates throughout the study area, which is particularly important because degree of saturation strongly influences electrical resistivity. Finally, incorporating additional factors that influence resistivity, such as total dissolved solids, may improve future transformations of resistivity to lithology.

6. REFERENCES

Aarhus GeoSoftware. (n.d.). *Getting started with SPIA TEM*. https://help.seequent.com/SPIA/en-GB/Content/Resources/DownloadableAssets/SPIA_TEM_manual ver 3.x.pdf

Auken, E., Foged, N., Larsen, J. J., Lassen, K. V. T., Maurya, P. K., Møller Dath, S., & Eiskjær, T. T. (2018). tTEM — A towed transient electromagnetic system for detailed 3D imaging of the top 70 m of the subsurface. *Geophysics, 84*(1), E13-E22. https://doi.org/10.1190/geo2018-0355.1

Baines, D., Smith, D. G., Froese, D. G., Bauman, P., & Nimeck, G. (2002). Electrical resistivity ground imaging (ERGI): A new tool for mapping the lithology and geometry of channel-belts and valley-fills. *Sedimentology, 49*(3), 441-449. https://doi.org/10.1046/j.1365-3091.2002.00453.x

Bouwer, H. (1977). Land Subsidence and Cracking Due to Ground-Water Depletion. *Groundwater, 15*, 358-364. https://doi.org/10.1111/j.1745-6584.1977.tb03180.x

Conway, B. D. (2016). Land subsidence and earth fissures in south-central and southern Arizona, USA. *Hydrogeology Journal, 24*(3), 649-655. https://doi.org/10.1007/s10040-015-1329-z

DuRoss, C. B., & Kirby, S. M. (2004). Reconnaissance investigation of ground cracks along the western margin of Parowan Valley, Iron County, Utah. Utah Geological Survey. https://ugspub.nr.utah.gov/publications/reports_of_investigations/ri-253.pdf

Esri. (2026). *Smooth interpolation*. ArcGIS Pro Documentation. https://doc.esri.com/en/arcgis-pro/latest/help/analysis/geostatistical-analyst/smooth-interpolation.html

Gorrie, C., Steelman, C. M., Conway-White, O., Smiarowski, A., Arnaud, E. & Parker, B. L. (2025). Generating a Statistically Constrained Quaternary Model of a Buried Bedrock Valley Using FDEM. *Groundwater, 63*, 351-370. https://doi.org/10.1111/gwat.13478

Guideline Geo. (2022). *ABEM WalkTEM 2 Onboard vs Desktop Processing in SPIA*. https://youtu.be/pGEg2FwpJEU?si=f0PzPkQhdJw5znFs

Hilton, A., & Jasechko, S. (2023). Widespread aquifer depressurization after a century of intensive groundwater use in USA. *Science Advances, 9*(37), eadh2992. https://doi.org/10.1126/sciadv.adh2992

King, A., & González-Álvarez, I. (2016). Integrated inversion of electromagnetic and geological data for regolith characterisation. *ASEG Extended Abstracts, 2016*(1), 1-5. https://doi.org/10.1071/ASEG2016ab297

Kirsch, R. (Ed.). (2009). *Groundwater Geophysics: A Tool for Hydrogeology* (2nd ed.). Springer. https://doi.org/10.1007/978-3-540-88405-7

Knight, R., Smith, R., Asch, T., Abraham, J., Cannia, J., Viezzoli, A., & Fogg, G. (2018). Mapping aquifer systems with airborne electromagnetics in the Central Valley of California. *Groundwater, 56*(6), 893-908. https://doi.org/10.1111/gwat.12656

Li, J., Smith, R., & Grote, K. (2023). Analyzing spatio-temporal mechanisms of land subsidence in the Parowan Valley, Utah, USA. *Hydrogeology Journal, 31*, 293-311. https://doi.org/10.1007/s10040-022-02583-5

Li, J., Smith, R., Grote, K., & Pedersen, J. B. (2024). Aquifer characterization using towed time domain electromagnetics in a variably saturated, data-sparse region. *Journal of Applied Geophysics, 228*, 105440. https://doi.org/10.1016/j.jappgeo.2024.105440

Marston, T. M. (2017). Water Resources of Parowan Valley, Iron County, Utah. *U.S. Geological Survey Scientific Investigations Report 2017-5033*. https://doi.org/10.3133/sir20175033

Maurya, P. K., Christiansen, A. V., Pedersen, J., & Auken, E. (2020). High resolution 3D subsurface mapping using a towed transient electromagnetic system - tTEM: case studies. *Near Surface Geophysics, 18*, 249-259. https://doi.org/10.1002/nsg.12094

McCarter, W. J. (1984). The electrical resistivity characteristics of compacted clays. *Geotechnique, 34*, 263-267. 10.1680/geot.1984.34.2.263.

Muhammad, S., Khalid, P., & Ehsan, M. I. (2022). Spatial appraisal of aquifer characterization through hydrogeophysical investigations in central part of Bari Doab, Punjab, Pakistan. *Environmental Monitoring and Assessment, 194*, 922. https://doi.org/10.1007/s10661-022-10645-0

Nugroho, H., Wikantika, K., Bijaksana, S., & Saepuloh, A. (2023). Integration of remote sensing and geophysical data to enhance lithological mapping utilizing the Random Forest classifier: a case study from Komopa, Papua Province, Indonesia. *Journal of Degraded and Mining Lands Management, 10*(3), 4417-4432. https://doi.org/10.15243/jdmlm.2023.103.4417

Olabode, O. P., & San, L. H. (2023). Analysis of soil electrical resistivity and hydraulic conductivity relationship for characterisation of lithology inducing slope instability in residual soil. *International Journal of Geo-Engineering, 14*, 7. https://doi.org/10.1186/s40703-023-00184-z

Sandersen, P. B. E., Kallesøe, A. J., Møller, I., Høyer, A. S., Jørgensen, F., Pedersen, J. B., & Christiansen, A. V. (2021). Utilizing the towed Transient ElectroMagnetic method (tTEM) for achieving unprecedented near-surface detail in geological mapping. *Engineering Geology, 288*, 106125. https://doi.org/10.1016/j.enggeo.2021.106125

Smith, R., & Li, J. (2021). Modeling elastic and inelastic pumping-induced deformation with incomplete water level records in Parowan Valley, Utah. *Journal of Hydrology, 601*, 126654. https://doi.org/10.1016/j.jhydrol.2021.126654

Smith, R., Li, J., Grote, K., & Butler, J. (2023). Estimating aquifer system storage loss with water levels, pumping and InSAR data in the Parowan Valley, Utah. *Water Resources Research, 59*, e2022WR034095. https://doi.org/10.1029/2022WR034095

APPENDIX A – SUPPLEMENTARY DATA

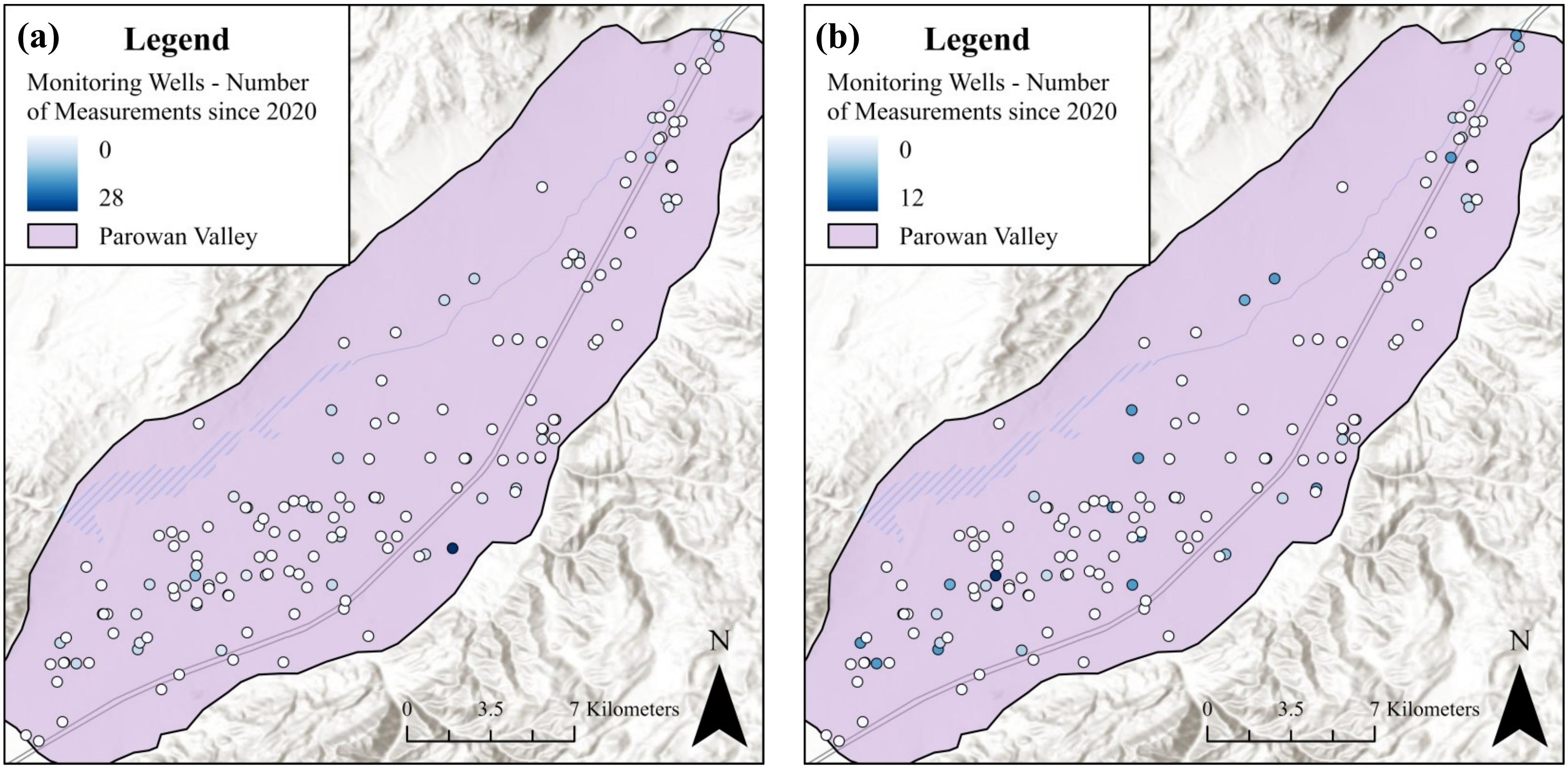

Figure A1: Monitoring Wells with Number of Measurements since 2020. (a) All monitoring wells. (b) Excluding the monitoring well with 28 measurements since 2020 to better visualize the spatial distribution.

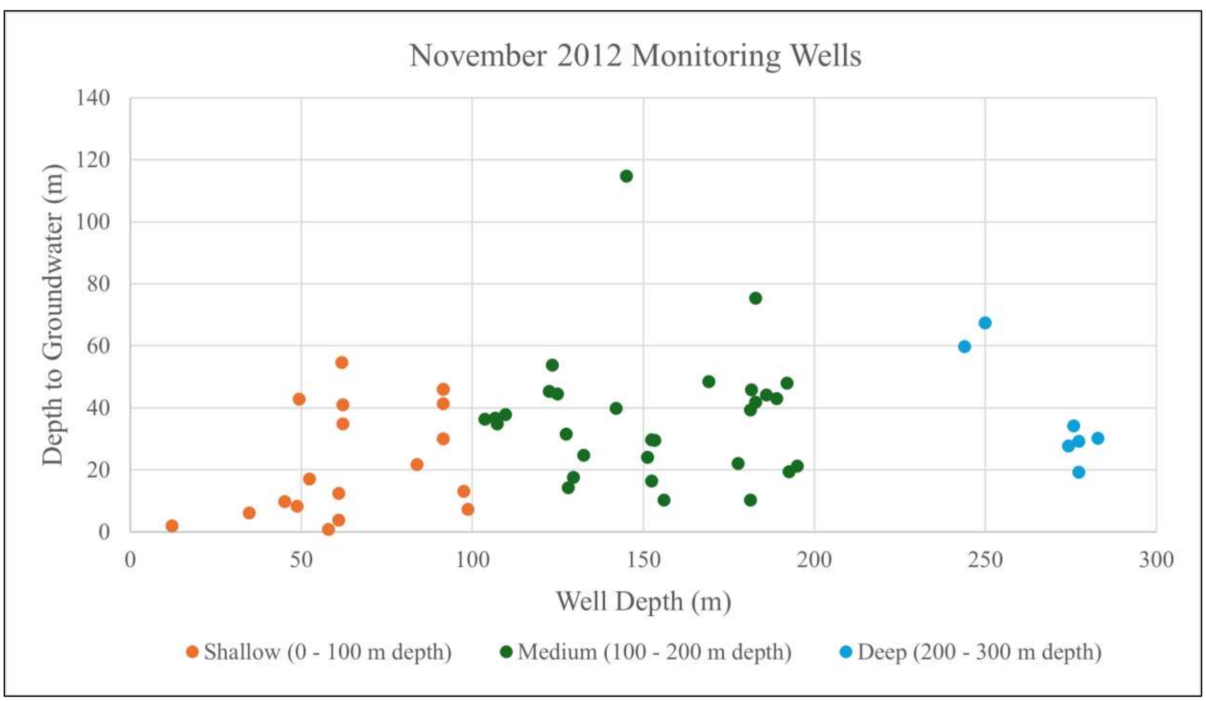

Figure A2: Depth to Groundwater vs. Well Depth for November 2012 Monitoring Wells

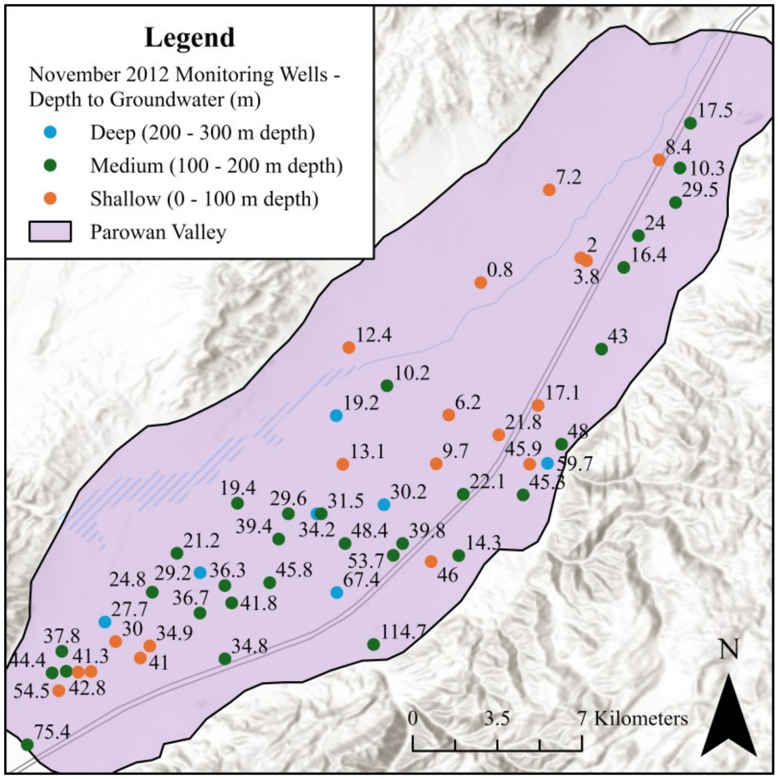

Figure A3: Depth to Groundwater for November 2012 Monitoring Wells

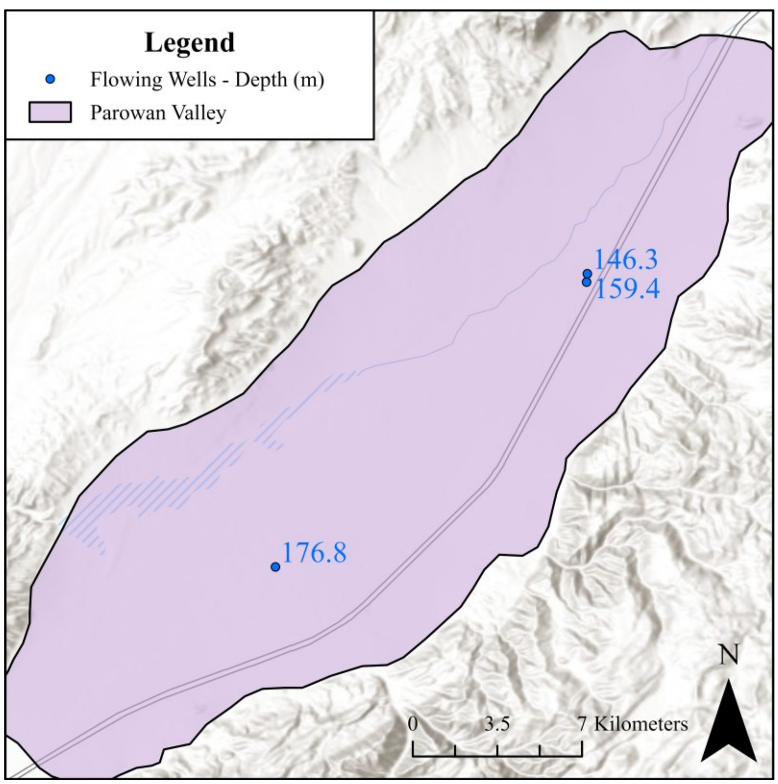

Figure A4: Flowing Wells

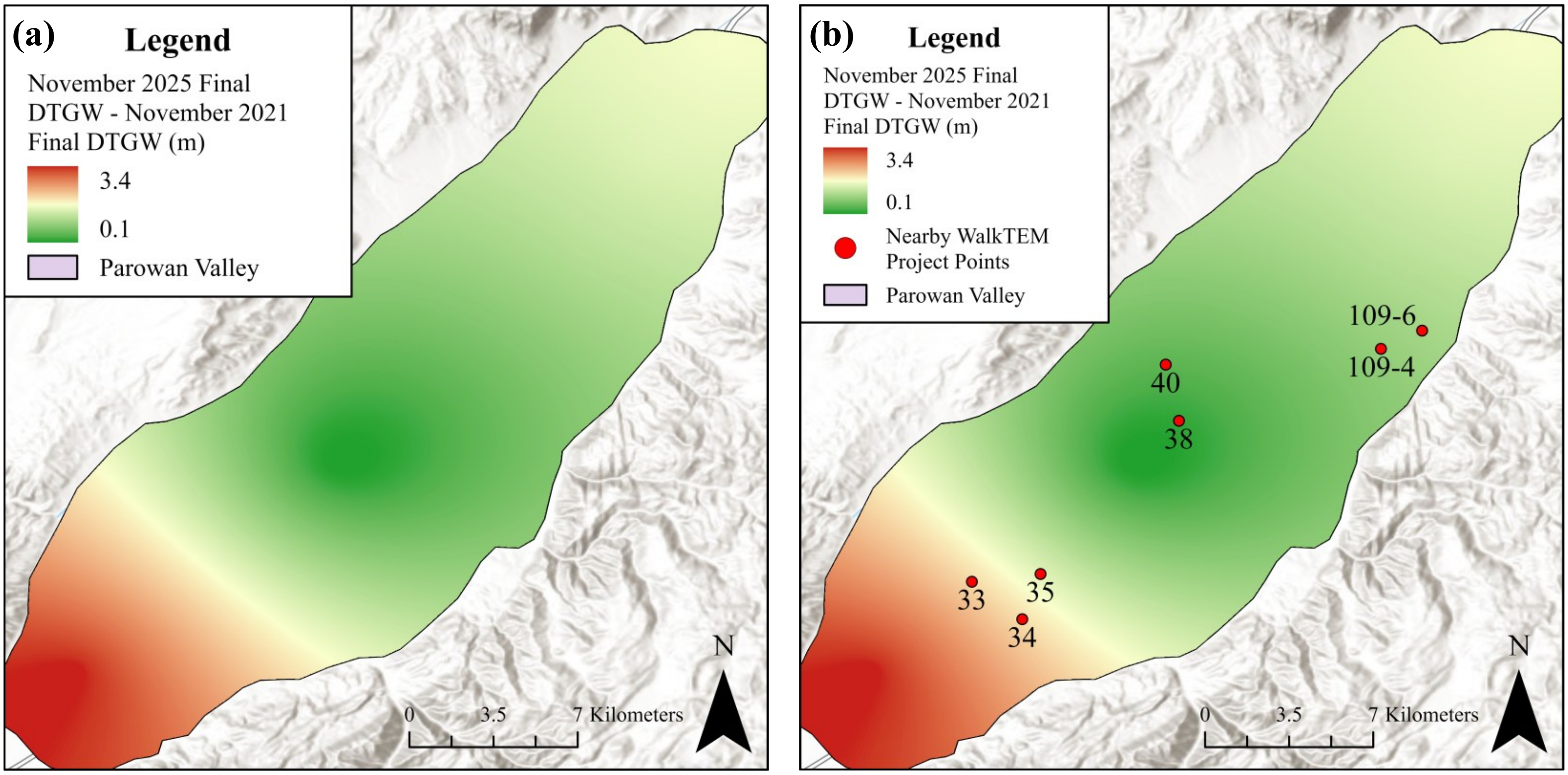

Figure A5: Difference Between November 2025 Final DTGW and November 2021 Final DTGW. (a) DTGW difference surface. (b) Including nearby WalkTEM project points.

Table A1: tTEM and WalkTEM Inversion Comparisons at Nearby Points

WalkTEM Project 35
Distance = 3.1 m

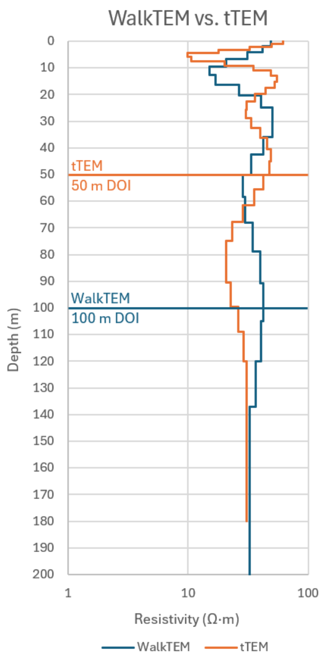

WalkTEM Project 109-4
Distance = 16.9 m

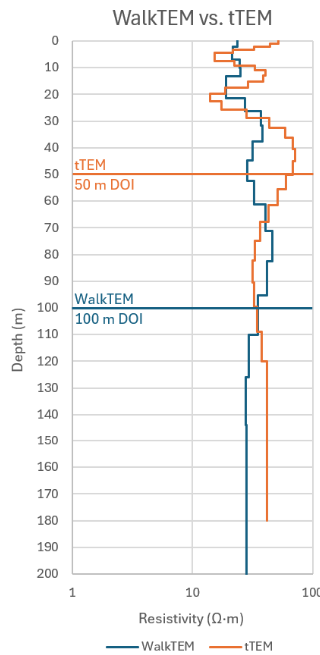

WalkTEM Project 40
Distance = 18.1 m

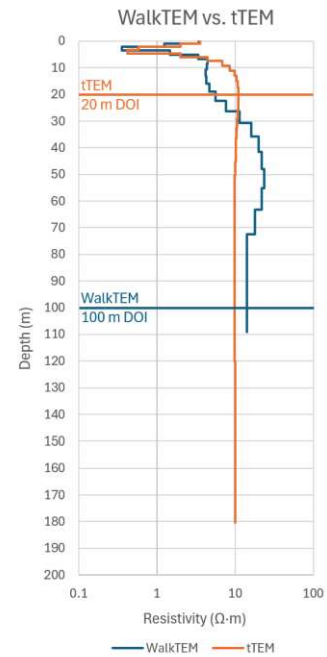

WalkTEM Project 38
Distance = 19.5 m

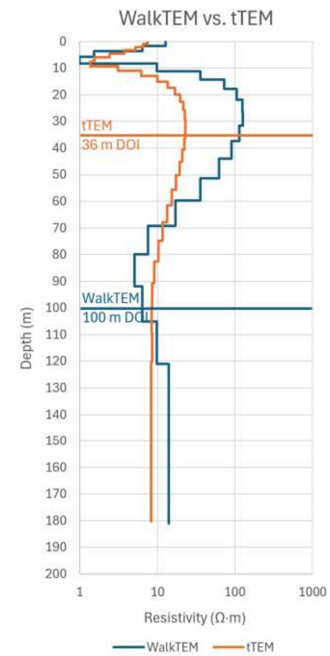

WalkTEM Project 109-6
Distance = 50.9 m

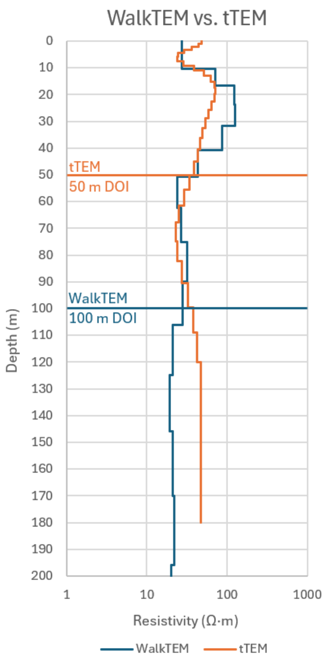

WalkTEM Project 33
Distance = 74.8 m

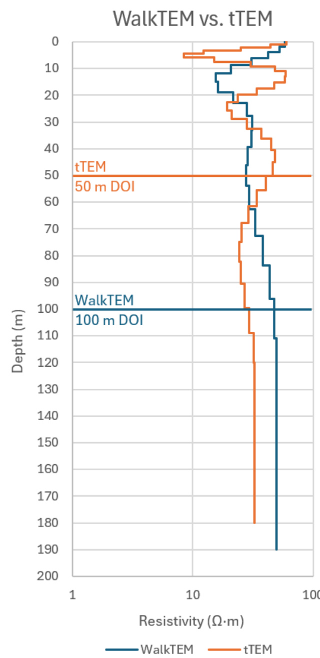

WalkTEM Project 34
Distance = 93.7 m

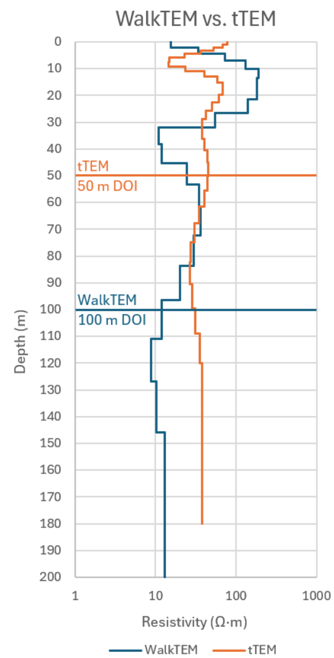

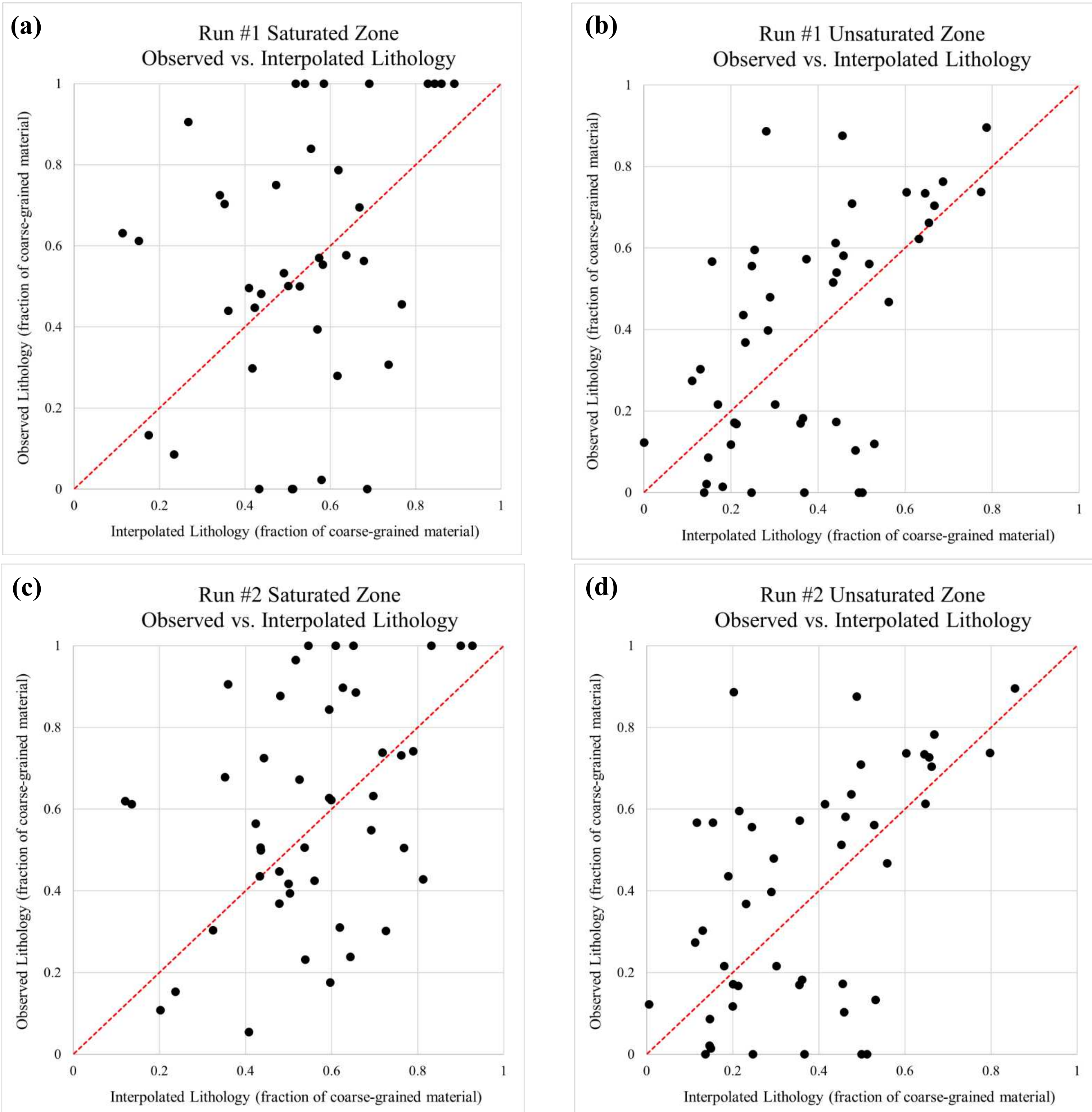
(a)
Run #1 Saturated Zone
Observed vs. Interpolated Lithology
Observed Lithology (fraction of coarse-grained material)
Interpolated Lithology (fraction of coarse-grained material)
(b)
Run #1 Unsaturated Zone
Observed vs. Interpolated Lithology
Observed Lithology (fraction of coarse-grained material)
Interpolated Lithology (fraction of coarse-grained material)
(c)
Run #2 Saturated Zone
Observed vs. Interpolated Lithology
Observed Lithology (fraction of coarse-grained material)
Interpolated Lithology (fraction of coarse-grained material)
(d)
Run #2 Unsaturated Zone
Observed vs. Interpolated Lithology
Observed Lithology (fraction of coarse-grained material)
Interpolated Lithology (fraction of coarse-grained material)

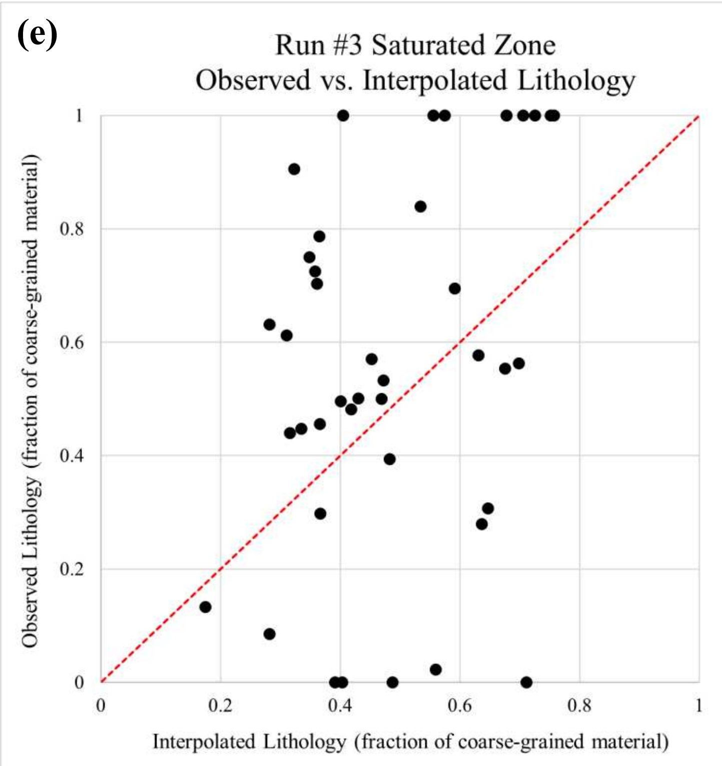

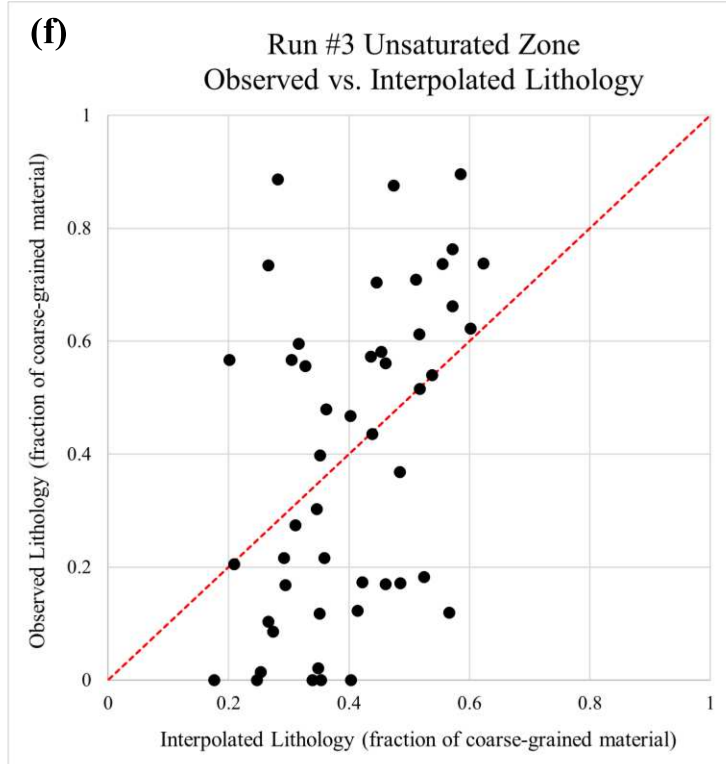

Figure A6: Observed vs. Interpolated Lithology Plots. (a) Run #1 Saturated Zone. (b) Run #1 Unsaturated Zone. (c) Run #2 Saturated Zone. (d) Run #2 Unsaturated Zone. (e) Run #3 Saturated Zone. (f) Run #3 Unsaturated Zone.

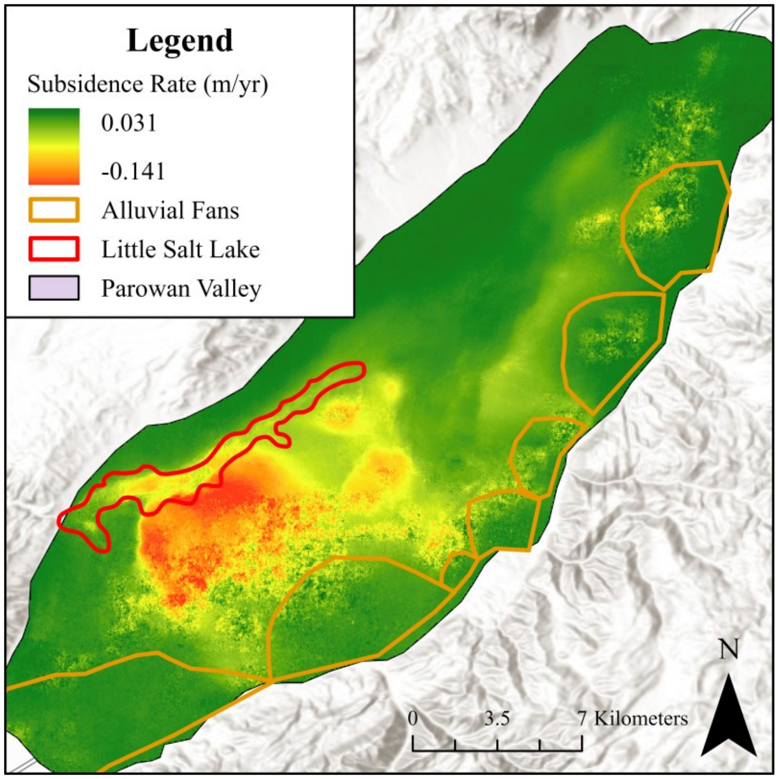

Figure A7: Land subsidence rate within Parowan Valley. Adapted from Li et al. (2023).

APPENDIX B – CALCULATIONS

Monitoring Well	Well Depth (m)	Well Depth Category	Date	Depth to Groundwater (m)	Distance to (C-31- 7)31acc- 1 (m)	March to November Difference (m)	Average March to November Difference (m)	Inverse Distance Weight	Normalized Inverse Distance Weight	Estimated November 2021 Water Level (m)	Estimated November 2025 Water Level (m)
(C-31- 7)31acc- 1	39.6	Shallow	March 2021	47.38						48.63	50.36
			March 2025	49.12							
(C-31- 7)31cca- 1	N/A	N/A	March 2012	32.76	919.7	1.30	1.30	0.001087	0.709		
			November 2012	34.07							
(C-32- 8)13bca- 1	48.8	Shallow	March 2012	7.71	5139.5	0.64	0.44	0.000195	0.127		
			November 2012	8.35							
			March 2013	8.00		0.25					
			November 2013	8.24							
			March 2021	11.18							
			March 2025	12.73							
(C-32- 8)24acb- 1	153.3	Medium	March 2012	27.49	6605.8	1.98	1.65	0.000151	0.099		
			November 2012	29.47							
			March 2013	28.31		1.32					
			November 2013	29.63							
			March 2021	32.25							
			March 2025	33.86							
(C-32- 8)27dca- 1	61.0	Shallow	March 2012	2.14	9921.7	1.65	1.61	0.000101	0.066		
			November 2012	3.80							
			March 2013	2.61		1.57					
			November 2013	4.18							
			March 2021	6.59							
			March 2025	7.81							

Sum	Seasonal Correction (m)
0.001534	1.25

Figure B1: Inverse Distance Weighting Calculations

Lithologic Dataset					
Drillers' Log	**Average Layer Thickness (m)**	**Drillers' Log**	**Average Layer Thickness (m)**	**Drillers' Log**	**Average Layer Thickness (m)**
458	17.4	13947	9.0	26185	4.5
460	8.5	13949	6.8	26389	9.9
806	114.6	13950	7.3	26727	5.8
1788	7.5	13959	11.1	26820	4.2
2802	5.7	13963	4.5	26908	5.8
2987	3.0	13964	3.6	27443	4.0
3381	8.9	13965	5.0	28180	7.5
5450	11.8	13981	2.8	28483	7.0
6252	7.0	13982	7.9	28518	19.0
6562	7.0	13983	11.3	28787	9.9
6745	3.3	13984	3.6	28966	3.4
7090	15.8	13987	21.2	29268	50.0
7344	12.4	13990	41.8	29700	9.9
7625	5.6	13991	4.9	30062	19.3
7766	3.2	13992	13.4	30092	11.5
8560	11.6	13993	3.9	30241	7.3
8680	4.2	13996	4.5	31856	3.8
9173	4.3	13997	10.9	32355	5.5
9205	107.6	13998	7.8	33631	7.2
9447	9.7	13999	14.1	34452	23.4
10248	30.2	14000	10.2	34643	10.9
10541	5.7	14002	11.9	34828	5.0
10587	9.9	14107	14.1	34962	4.3
10791	5.1	14648	3.9	35082	14.0
11392	7.5	14660	4.5	35142	22.1
11431	5.0	14809	4.6	35143	7.3
11719	8.5	15018	11.0	35544	17.5
11730	6.3	15019	16.5	35557	6.6
11738	11.8	15348	22.1	123500	23.2
11776	6.4	15526	21.8	426887	5.4
11857	12.3	15854	11.0	427208	12.0
12119	6.3	16006	6.7	428352	3.8
12152	13.8	16010	5.1	429392	5.1
12196	6.7	16389	4.6	429619	17.7
12268	11.8	16533	110.6	429702	9.1
12421	10.1	16747	29.2	429870	25.9
13587	8.6	16812	6.2	430072	7.0
13856	2.0	17425	8.6	430080	7.7
13859	3.4	17888	4.2	430198	5.2
13869	2.3	18619	76.2	430313	3.1
13870	3.0	18717	66.0	430589	4.2
13886	4.4	19178	3.8	430907	5.6
13887	4.8	19378	10.6	431036	33.4
13888	6.6	19769	1.6	431072	5.8
13903	4.4	19770	2.0	431118	5.1
13907	8.1	19771	2.5	431341	15.2
13908	4.5	19786	14.0	437658	68.3
13909	5.3	20075	22.2	440512	70.1
13910	3.3	20763	4.6	441562	22.4
13911	6.7	21679	14.0	443389	16.8
13912	11.0	21757	5.5	1234999	5.0
13913	3.7	22137	7.0	0375002P00 27210	4.4
13914	8.5	23191	4.2	0475001M00 29647	1.4
13915	3.9	23197	5.5	0475001M00 29648	1.1
13916	10.8	23280	5.8	0675001M00 428859	2.6
13918	6.9	23342	8.9	0775001M00 429706	6.1
13923	13.1	23427	7.0	0875002M00 432174	2.1
13924	3.4	23655	4.9	0875002M00 432175	2.3
13926	4.0	23946	6.8	0975001M00 433013	50.3
13928	16.0	24028	8.5	0975002M00 433344	8.1
13940	24.5	24196	4.9	1075001M00 434217	1.8
13943	30.5	24540	7.6	1075001M00 434218	4.9
13944	7.4	25010	7.4	1075001M00 434219	4.5
13945	14.7	25423	3.0	1475001M00 437740	11.8
13946	19.2	25556	6.8	Average Layer Thickness (m)	12.2

Figure B2: Average Layer Thickness Calculations for Lithologic Dataset

tTEM Dataset		
Top Depth	**Bottom Depth**	**Thickness (m)**
3.3	4.6	1.3
4.6	6.0	1.4
6.0	7.5	1.5
7.5	9.2	1.7
9.2	11.0	1.8
11.0	12.9	2.0
12.9	15.1	2.1
15.1	17.4	2.3
17.4	19.9	2.5
19.9	22.7	2.8
22.7	25.7	3.0
25.7	28.9	3.3
28.9	32.5	3.6
32.5	36.3	3.9
36.3	40.5	4.2
40.5	45.1	4.6
45.1	50.1	5.0
50.1	55.5	5.4
55.5	61.4	5.9
61.4	67.8	6.4
Average Layer Thickness (m)		3.2

WalkTEM Dataset	
Project	**Average Layer Thickness (m)**
26	6.0
27	7.0
28	6.3
30	5.1
31	5.3
33	5.3
35	5.3
36	5.8
37	1.9
38	5.0
39	5.4
40	4.3
41	5.2
42	6.1
44	4.9
45	6.3
46	6.2
108-3	6.4
108-9	7.5
108-11	7.8
108-14	7.5
108-18	7.3
109-2	9.5
109-4	5.3
109-6	8.4
110	4.8
111	8.2
112	4.6
Average Layer Thickness (m)	6.0

Figure B3: Average Layer Thickness Calculations for Geophysical Datasets

$$\bar{x} = \frac{\sum_{i=1}^{n} x_i \times w_i}{\sum_{i=1}^{n} w_i} = \frac{(1 \times 30\ m) + (0 \times 25\ m) + (1 \times 65\ m) + (0.5 \times 63\ m) + (0 \times 35\ m) + (0.5 \times 106) + (1 \times 56\ m)}{30\ m + 25\ m + 65\ m + 63\ m + 35\ m + 106\ m + 56\ m} = 0.62$$

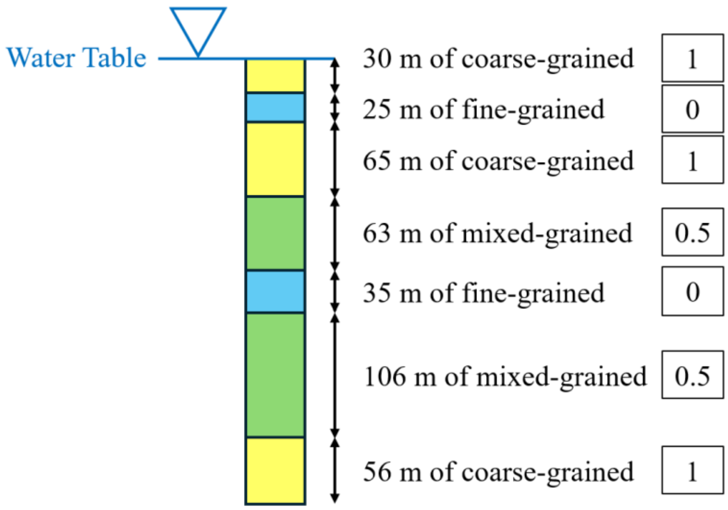

Lithology Classification	Value
Coarse-grained	1
Mixed-grained	0.5
Fine-grained	0

Figure B4: Example Lithology Weighted Average Calculation

APPENDIX C – WELL LOGS AND FIELD NOTES

Utah Division of Water Rights

WELLPRT Well Log Information Listing

Version: 2003.09.18.00 Rundate: 10/12/2003 03:58 PM

Utah Division of Water Rights

Water Well Log

LOCATION:
S 200 ft W 1320 ft from NE CORNER of SECTION 34 T 32S R 8W BASE SL Elevation: feet

DRILLER ACTIVITIES:
ACTIVITY # 1 NEW WELL
DRILLER: THAYER WELL DRILLING LICENSE #: 661
START DATE: 12/23/2000 COMPLETION DATE: 03/06/2001

BOREHOLE INFORMATION:

Depth(ft) From	To	Diameter(in)	Drilling Method	Drilling Fluid
0	30	13	CABLE TOOL	WATER
30	80	11	CABLE TOOL	WATER
80	480	8	CABLE TOOL	

LITHOLOGY:

Depth(ft) From	To	Lithologic Description	Color	Rock Type
0	17	LOW-PERMEABILITY,CLAY,SILT,SAND	BROWN	
17	35	LOW-PERMEABILITY,CLAY,SILT	BROWN	
35	42	WATER-BEARING,LOW-PERMEABILITY,CLAY CRUMBLY CLAY	BROWN	
42	85	WATER-BEARING,LOW-PERMEABILITY,CLAY CRUMBLY CLAY	RED BROWN	
85	91	LOW-PERMEABILITY,CLAY,SILT,SAND SOFT FINE GRAINED	BROWN	
91	95	HIGH-PERMEABILITY,SILT,SAND	BROWN	
95	107	LOW-PERMEABILITY,CLAY,GRAVEL	BROWN	
107	130	LOW-PERMEABILITY,CLAY	GRAY	
130	144	LOW-PERMEABILITY,CLAY	TAN	
144	170	LOW-PERMEABILITY,CLAY,SILT SOFT	BROWN	
170	201	LOW-PERMEABILITY,CLAY,SAND,GRAVEL SMALL AND SAND GRAVEL MIXED IN		
201	203	WATER-BEARING,HIGH-PERMEABILITY,SAND	BLACK	
203	205	WATER-BEARING,HIGH-PERMEABILITY,SAND,GRAVEL	BLACK	
205	213	LOW-PERMEABILITY,SILT,SAND APPEARS TO BE DRY SANDSTONE FINE	BROWN BLACK	
213	215	WATER-BEARING,HIGH-PERMEABILITY,SAND,GRAVEL		
215	221	LOW-PERMEABILITY,CLAY	BROWN	
221	224	WATER-BEARING,HIGH-PERMEABILITY,SAND	BLACK	
224	249			
249	283	LOW-PERMEABILITY	BROWN	
283	302	LOW-PERMEABILITY,CLAY,SILT FINE GRAINED		
302	310	LOW-PERMEABILITY,CLAY,SILT MORE CLAY, LESS SAND	BROWN	
310	330	LOW-PERMEABILITY,SAND	BLACK	

Figure C1: WIN 23191 Drillers' Log Page 1

		FINE GRAINED		
		SANDSTONE- BRITTLE		
330	338	CLAY,SILT	BROWN	
		TOUGH		
338	347	WATER-BEARING,SAND,GRAVEL	BLACK	
347	368	LOW-PERMEABILITY,CLAY,SILT,SAND,GRAVEL	BROWN	
		343 347 CLAY, TOUGH		
		2" T		
368	372	WATER-BEARING,SILT,GRAVEL		
		DIRTY LOOKING NOT MUCH WATER		
372	402	LOW-PERMEABILITY,CLAY,SAND		
		MOSTLY CLAY		
402	405	LOW-PERMEABILITY,CLAY,GRAVEL	BROWN	
405	415	LOW-PERMEABILITY,CLAY,SAND,GRAVEL	BROWN	
415	421	LOW-PERMEABILITY,CLAY	BROWN	
		TOUGH		
421	427	WATER-BEARING,HIGH-PERMEABILITY,SAND,GRAVEL	BLACK	VOLCANIC
		GOOD STUFF - CLEAN		
427	444	LOW-PERMEABILITY,CLAY,SAND,GRAVEL		
		MOSTLY CLAY, WITH SALT SPOTS		
444	448	LOW-PERMEABILITY,CLAY		
		TOUGH		
448	455	WATER-BEARING,SAND,GRAVEL	BLACK	VOLCANIC
		VERY CLEAN, HARD TO DRILL		
455	470	LOW-PERMEABILITY,CLAY,SAND		
470	475	WATER-BEARING,SAND,GRAVEL		
475	478	LOW-PERMEABILITY,CLAY	BROWN	

WATER LEVEL DATA:

Date	Time	Water Level (feet) (-)above ground	Status
03/06/2001		.00	FLOWING

CONSTRUCTION - CASING:

Depth(ft) From	To	Material	Gage(in)	Diameter(in)
0	480	A53B	.250	8

CONSTRUCTION - SCREENS/PERFORATIONS:

Depth(ft) From	To	Screen(S) or Perforation(P)	Slot/Perf. siz	Screen Diam/Length Perf(in)	Screen Type/# Perf.
422	430	PERFORATION			75
430	440	PERFORATION			30
450	457	PERFORATION			100
471	475	PERFORATION			41

CONSTRUCTION - FILTER PACK/ANNULAR SEALS

Depth(ft) From	To	Material	Amount	Density(pcf)
0	78	GROUT	12 BG MX	
78	80	BEN CHIPS	1 BAG	

WELL TESTS:

Date	Test Method	Yield (CFS)	Drawdown (ft)	Time Pumped (hrs)
03/01/2001	BAILER	.111	17	6

GENERAL COMMENTS:

CONSTRUCTION INFORMATION:
Well Head Configuration: Capped
Perforator used: mills knife
Surface Seal: yes
Depth 50 feet
Drive Shoe: yes
Material Placement Method; trimmie
Comments: I pulled off this well to drill monitor wells that had
critical time
Went back todrill and the weather was awful
ADDITIONAL DATA NOT AVAILABLE

Figure C2: WIN 23191 Drillers' Log Page 2

Utah Division of Water Rights

WELLPRT Well Log Information Listing

Version: 2003.09.18.00 Rundate: 10/13/2003 06:31 AM

Utah Division of Water Rights

Water Well Log

LOCATION:
S 2440 ft W 65 ft from N4 CORNER of SECTION 3 T 34S R 9W BASE SL Elevation: feet

DRILLER ACTIVITIES:
ACTIVITY # 1 WELL ABANDONMENT
DRILLER: ANZALONE WELL SERVICE LICENSE #: 749
START DATE: / / COMPLETION DATE: / /
ACTIVITY # 2 WELL REPLACEMENT
DRILLER: ANZALONE WELL SERVICE LICENSE #: 749
START DATE: 03/20/2003 COMPLETION DATE: 04/30/2003

BOREHOLE INFORMATION:

Depth(ft) From	Depth(ft) To	Diameter(in)	Drilling Method	Drilling Fluid
0	580	24	MUD ROTARY	BENTONITE

LITHOLOGY:

Depth(ft) From	Depth(ft) To	Lithologic Description	Color	Rock Type
0	20	CLAY,SILT,SAND		
20	30	CLAY		
30	60	SAND,GRAVEL		
60	90	CLAY,SILT,SAND,GRAVEL		
90	105	CLAY,SILT		
105	140	SAND,GRAVEL,COBBLES		
140	150	CLAY		
150	165	SAND,GRAVEL		
165	175	CLAY		
175	200	SAND,GRAVEL,COBBLES		
200	207	CLAY		
207	230	SILT,SAND,GRAVEL		
230	240	CLAY		
240	260	SAND,GRAVEL		
260	264	CLAY		
264	300	SAND,GRAVEL		
300	365	CLAY		
365	400	SILT,SAND,GRAVEL		
400	415	CLAY,SILT		
415	460	SAND,GRAVEL		
460	465	CLAY		
465	490	SAND,GRAVEL		
490	530	CLAY,SILT		
530	540	GRAVEL		
540	580	CLAY,SILT,SAND,GRAVEL		

WATER LEVEL DATA:

Date	Time	Water Level (feet) (-)above ground	Status
03/27/2003		164.00	FLOWING

Figure C3: WIN 26908 Drillers' Log Page 1

CONSTRUCTION - CASING:

Depth(ft) From	To	Material	Gage(in)	Diameter(in)
0	180	STEEL A53B	.312	16

CONSTRUCTION - SCREENS/PERFORATIONS:

Depth(ft) From	To	Screen(S) or Perforation(P)	Slot/Perf. siz	Screen Diam/Length Perf(in)	Screen Type/# Perf.
180	580	PERFORATION	.16	3	16 ROW

CONSTRUCTION - FILTER PACK/ANNULAR SEALS

Depth(ft) From	To	Material	Amount	Density(pcf)
0	35	CONCRETE	4CU YDS	8
35	580	3/8 WASHED GRAVEL	38 CU YD	

WELL TESTS:

Date	Test Method	Yield (CFS)	Drawdown (ft)	Time Pumped (hrs)
03/27/2003	AIR DEVELOPMENT	.891		6
04/10/2003	TEST PUMP	4.902	52	30

GENERAL COMMENTS:

CONSTRUCTION INFORMATION
Well Head Configuration: Turbine Discharge head
Casing Joint Type: Welded - 2 pass
Perforator Used: Factory Mill
Surface Seal: Yes
Depth of Surface Seal: 35 Feet
Drive Shoe: No
Surface Seal Placement Method: Poured
Pump Desc. Line Shaft Turbines
Horsepower: 200
Pump Intake Depth: 265 Feet
Approx. Pumping Rate: 1900 GPM
Well Disinfected: Yes
Location: N. W. of Parowan
Additional Information Not Available

Figure C4: WIN 26908 Drillers' Log Page 2

Utah Division of Water Rights

WELLPRT Well Log Information Listing

Version: 2003.09.18.00 **Rundate: 10/13/2003 07:30 AM**

Utah Division of Water Rights

Water Well Log

LOCATION:
S 1184 ft W 1399 ft from NE CORNER of SECTION 34 T 32S R 8W BASE SL Elevation: feet

DRILLER ACTIVITIES:
ACTIVITY # 1 WELL REPAIR
DRILLER: THAYER WELL DRILLING LICENSE #: 661
START DATE: 04/28/2003 COMPLETION DATE: 05/02/2003

BOREHOLE INFORMATION:

Depth(ft) From	To	Diameter(in)	Drilling Method	Drilling Fluid
418	523	8	CABLE TOOL	FORMATION

LITHOLOGY:

Depth(ft) From	To	Lithologic Description	Color	Rock Type
478	498	LOW-PERMEABILITY,CLAY		
498	520	SAND,GRAVEL		
520	823	CLAY		

WATER LEVEL DATA:

Date	Time	Water Level (feet) (-)above ground	Status
05/02/2003		.00	FLOWING

CONSTRUCTION - CASING:

Depth(ft) From	To	Material	Gage(in)	Diameter(in)
470	523	A53B STEEL	.250	6

CONSTRUCTION - SCREENS/PERFORATIONS:

Depth(ft) From	To	Screen(S) or Perforation(P)	Slot/Perf. siz	Screen Diam/Length Perf(in)	Screen Type/# Perf.
503	523	PERFORATION	.13	3	24

WELL TESTS:

Date	Test Method	Yield (CFS)	Drawdown (ft)	Time Pumped (hrs)
/ /	BAILER	.000		

GENERAL COMMENTS:
CONSTRUCTION INFORMATION
Well Head Configuration: No Data
Casing Joint Type: Welded
Perforator Used: Factory Perfs
Surface Seal: No
Depth of Surface Seal: No Data
Drive Shoe: No - Banded Eash End
Surface Seal Placement Method: No Data

Figure C5: WIN 27164 Drillers' Log

Table C1: Field Notes for Excluded WalkTEM Project Points

WalkTEM Project	Data Residual	Field Notes	Possible Contributing Factors
32	4.68	• Wet ground conditions from rain	Possible unmodeled subsurface effects such as induced polarization
34	3.14	• Wet ground conditions from rain • Thick alfalfa prevented proper loop placement on the ground o Loops instead rested on top of vegetation • Adjacent to a center pivot	Possible coupling / infrastructure interference
43	2.26	• Adjacent to an airport and construction site • Thick sagebrush prevented proper loop geometry on the ground	Possible infrastructure interference / geometry effects
47	4.36	• Tried switching the silver cable connecting the WalkTEM and transmitter, but results did not improve • Twist / spiral observed in one receiver cable	Possible instrument / cable noise
48	4.45	• Thick sagebrush prevented proper loop geometry on the ground	Possible geometry effects